JOURNAL OF GEOPHYSICAL RESEARCH, VOL. 105, NO. E9, PAGES 22,559–22,578, SEPTEMBER 25, 2000

Geologic mapping of Europa

Ronald Greeley,[1] Patricio H. Figueredo,[1] David A. Williams,[1] Frank C. Chuang,[1] James E. Klemaszewski,[1] Steven D. Kadel,[1] Louise M. Prockter,[2] Robert T. Pappalardo,[2] James W. Head III,[2] Geoffrey C. Collins,[2] Nicole A. Spaun,[2] Robert J. Sullivan,[3] Jeffrey M. Moore,[4] David A. Senske,[5] B. Randall Tufts,[6] Torrence V. Johnson,[5] Michael J. S. Belton,[7] and Kenneth L. Tanaka[8]

Abstract. Galileo data enable the major geological units, structures, and surface features to be identified on Europa. These include five primary units (plains, chaos, band, ridge, and crater materials) and their subunits, along with various tectonic structures such as faults. Plains units are the most widespread. Ridged plains material spans a wide range of geological ages, including the oldest recognizable features on Europa, and appears to represent a style of tectonic resurfacing, rather than cryovolcanism. Smooth plains material typically embays other terrains and units, possibly as a type of fluid emplacement, and is among the youngest material units observed. At global scales, plains are typically mapped as undifferentiated plains material, although in some areas differences can be discerned in the near infrared which might be related to differences in ice grain size. Chaos material is composed of plains and other preexisting materials that have been severely disrupted by inferred internal activity; chaos is characterized by blocks of icy material set in a hummocky matrix. Band material is arrayed in linear, curvilinear, wedge-shaped, or cuspate zones with contrasting albedo and surface textures with respect to the surrounding terrain. Bilateral symmetry observed in some bands and the relationships with the surrounding units suggest that band material forms by the lithosphere fracturing, spreading apart, and infilling with material derived from the subsurface. Ridge material is mapped as a unit on local and some regional maps but shown with symbols at global scales. Ridge material includes single ridges, doublet ridges, and ridge complexes. Ridge materials are considered to represent tectonic processes, possibly accompanied by the extrusion or intrusion of subsurface materials, such as diapirs. The tectonic processes might be related to tidal flexing of the icy lithosphere on diurnal or longer timescales. Crater materials include various interior (smooth central, rough inner, and annular massif) and exterior (continuous ejecta) subunits. Structural features and landforms are shown with conventional symbols. Type localities for the units are identified, along with suggestions for portraying the features on geological maps, including colors and letter abbreviations for material units. Implementing these suggestions by the planetary mapping community would facilitate comparisons of maps for different parts of Europa and contribute to an eventual global synthesis of its complex geology. On the basis of initial mapping results, a stratigraphic sequence is suggested in which ridged plains form the oldest unit on Europa, followed by development of band material and individual ridges. Band materials tend to be somewhat older than ridges, but in many areas the two units formed simultaneously. Similarly, the formation of most chaos follows the development of ridged plains; although chaos is among the youngest materials on Europa, some chaos units might have formed contemporaneously with ridged plains. Smooth plains generally embay all other units and are late-stage in the evolution of the surface. C1 craters are superposed on ridged plains but are crosscut by other materials, including bands and ridges. Most c2 craters postdate all other units, but a few c2 craters are cut by ridge material. C3 craters constitute the youngest recognizable material on Europa.

[1]Department of Geology, Arizona State University, Tempe.
[2]Department of Geological Sciences, Brown University, Providence, Rhode Island.
Center for Radiophysics and Space Physics, Cornell University, Ithaca, New York.
[4]NASA Ames Research Center, Moffett Field, California.
[5]NASA Jet Propulsion Laboratory, Pasadena, California.
[6]Lunar and Planetary Laboratory, University of Arizona, Tucson.
[7]National Optical Astronomy Observatories, Tucson, Arizona.
[8]U.S. Geological Survey, Flagstaff, Arizona.

Paper number 1999JE001173.
0148-0227/00/1999JE001173$09.00

1. Introduction

The first spacecraft images of Europa were returned from the Voyager mission in 1979 [*Smith et al.*, 1979a, b]. Although the best resolution was only ~ 1.9 km/pixel and the coverage was incomplete, Voyager data enabled an assessment of Europa's geology when combined with Earth-based remote sensing of the surface. *Lucchitta and Soderblom* [1982] described the general geology of Europa and published a preliminary terrain map, which outlined the principal surface units. Subsequent studies of Europa based on Voyager data focused on specific features, such

as the various structural features [*Lucchitta et al.*, 1981], and the potential non-ice components of the surface. *Malin and Pieri* [1986] updated and reviewed the general geology of Europa, but no additional terrain or geologic mapping was carried out, primarily because of limitations in image resolution and coverage.

The Galileo spacecraft was placed in orbit around Jupiter in 1995, where it has made repeated flybys of the Galilean satellites (Plate. 1; Table 1). During the primary phase of the mission, there were nine orbits that returned images of Europa with resolutions as high as 20 m/pixel. Preliminary geological results from the imaging experiment are given by *Belton et al.* [1996], *Greeley* [1997], and *Greeley et al.* [1998]. During the Galileo Europa Mission, or extended phase (GEM), there were nine additional orbits returning images of Europa, some at ~6-10 m/pixel. In the future the Cassini spacecraft might image Europa at global-scale resolution (tens of km/pixel) during its flyby to Saturn. Thus, except for this anticipated coverage, all of the spacecraft data for Europa are on the ground until the next mission to the Jovian system is flown, currently expected to be the Europa Orbiter Mission, to be launched in the future.

During the primary and GEM phases of the Galileo mission, two imaging team workshops were held to discuss geological mapping of Europa using the new Galileo data. Preliminary geological maps [e.g., *Senske et al.*, 1998; *Prockter et al.*, 1999a] were prepared for regions of Europa as the data became available. These maps ranged from regional-scale compilations based on images with resolutions of a few hundred meters or more to local maps using images with resolutions of a few tens of meters. The preparation of these maps was guided by standard methods developed and described by e.g., *Shoemaker and Hackman* [1962], *Wilhelms* [1972, 1990], *Tanaka et al.* [1994] for mapping the geology of planetary surfaces.

The basic premise of geologic mapping is that units are composed of three-dimensional materials (i.e., they have thicknesses that extend below the surface) which can be placed in a stratigraphic position relative to other units and structuresolution Units are usually shown by colors or patterns on geological maps. Structures (such as faults and fractures) represent deformation or alteration of the geologic units in response to tectonic or other processes and are typically shown on maps by various symbols. In some cases, structures are so distinctive or characteristic of a terrain that they are used as part of the defining characteristics of the unit, although every effort is made to distinguish between the material properties of a unit and the superposed structure. One of the controversies in planetary mapping is distinguishing among geologic, physiographic, and surficial geologic portrayals [*Spudis and Greeley*, 1976] and the use of geomorphology to characterize geologic units. The convention proposed for mapping Europa follows that of *Wilhelms* [1990] for mapping icy satellites; if a region is so extensively modified by inferred tectonic processes that it no longer has its original properties, then it is treated as a new geologic unit. The terrestrial analogy would be selecting a sedimentary rock that has been extensively brecciated by tectonism and mapping it as a separate unit. The term tectonic resurfacing was adapted by *Head et al.* [1997] for Ganymede, and we suggest its application to parts of Europa.

In planetary geological mapping, the approach is to map and describe the units and structures on the basis of objective characteristics (e.g., surface textures, colors, relative albedos, etc.). The interpretation of the origin and evolution of units and structures is separated from the objective descriptions. In principle, the objective descriptions should be valid for any given set of data, but the interpretations are subject to change. From the geometry of the units and structural features, the style and timing of unit formation and deformation can be determined. Once maps have been compiled and the results have been synthesized, it is possible to derive a geological history for the area on the basis of stratigraphic principles, which is the ultimate goal of the mapping. In section 5 of this report we discuss some of the initial scientific results from the mapping of Europa.

The convention in planetary mapping is to divide planetary surfaces into quadrangles of consistent scales, which then serve as base maps for geological mapping. Scales typically range from 1:250,000 for small areas, such as landing sites on Mars, to global maps at 1:10,000,000 or less. Systematic geological mapping was conducted for some Galilean satellites at 1:5,000,000 on the basis of Voyager images. Such a scale is recommended for Europa, as base maps become available. It should be noted, however, that Galileo coverage and image resolution is highly variable for Europa (Plate 1), and that systematic mapping at a consistent scale will not be possible until more data are obtained.

In order to systematize the approach for mapping the geology of Europa, we have synthesized lessons learned from previous individual mapping projects, describing the major units (and their type localities) and the various structural features visible on the surface. Where possible, we have incorporated the original units and surface features presented by *Lucchitta and Soderblom* [1982]. Our goal is to provide suggested guidelines for mapping Europa, while presenting type examples and descriptions of Europa's primary units, subunits, and structuresolution This is a preliminary compilation, and it is likely that as more planetary scientists work with the data and as more insight into Europa is obtained, some of the concepts for units and structures will evolve.

2. Material Units

On the basis of Voyager images, *Lucchitta and Soderblom* [1982] defined five primary material units and terrains for Europa: plains material, mottled terrain, craters, band material, and "spots and bands." Subunits of these were defined primarily by differences in albedo or color (e.g., gray versus light band material, brown versus gray mottled terrain). When studied on the higher-resolution Galileo images, some of these units can be retained for mapping, while others need to be redefined or deleted. For example, mottled terrain was accurately described on Voyager data but is seen in high resolution to consist of diverse units and terrains. Some dark areas (comprising the "mottling") are parts of the icy lithosphere that have been

Plate 1. Map of Europa showing imaging coverage obtained during the Galileo mission.

Table 1. Galileo Image Coverage and Resolution of Europa

Orbit	Frames (Full and Partial)	Resolution (per Pixel)	Center Coordinates	Notes
G1	4 full	1.6 km	+35, 218	Vgr gap fill, six-color sample of polar terrain, best regional view of either pole during nominal mission
	1 240 lines	1.6 km	+19, 192	
	4 full [green, violet, 756, 968]	1.6 km	+47, 220	
	2 376 lines [red, 889]	1.6 km	+47, 221	
G2	3 color frames (returned 640x640 pxl window of each) [green, violet, 968]	6.9 km	0, 292	low phase photometry in violet, green, 968
C3	4 partial (535,40,225,96 lines)	0.43 km	-15, 195	wedge-shaped bands, Thera Macula, dark lineae, transition of plains unit to fracutred plains uit, terminator view for morphology
	1 40 lines	0.85 km	5, 190	
E4	5 (800,664,664,664, and 536 lines)	1.2 km	0, 280	terminator coverage, large macula, dark terrain at high resolution
	1 400 lines	0.63 km	6, 323	
	3 (2 x 400, and 275 lines)	0.13 km	-16, 334	
	4 partial (16-800 lines)	0.03 km	6, 323	
	4 partial (392-800 lines)	0.03 km	6, 327	
E6	2 full	1.7 km	-4, 242	Thera and Thrace Macula, Agenor Linea, plains, triple band intersection, strat relationships, "iceberg" chaos, bright plains at high resolution.
	2 full	0.28 km	-25, 272	
	6 full	0.18 km	12, 271	
	6 (2 at 400, 200, 3 at 125 lines)	0 052 km	13, 273	
G7	1 full	3.2 km	0, 149	Vgr gap fill, low and very low phase Photometry, Tyre Macula in green, violet, and 968, near terminator morphology
	6 370 lines [green, violet, 968]	0.4 km	36, 183	
	3 400 lines [green, violet, 968]	0.7 km	31, 147	
	5 (4 full and 1 at 25 lines)	0.5 km	2, 98	
C9	3-color [green, 756, 889]	12.6 km	0, 40	global color in green (no OCM), violet, and 968 - leading hemisphere, links to C10
C10	3-color [green] [violet, 968]	7.1 km	0, 283	global color in green (IM8), violet and 968 - trailing hemisphere, links to C3, E4, and C9
E11	5-color [green, violet, 756, 968, 889]	0.30 km	-2, 225	samples dark spot, Pwyll ray, wedge- shaped band
	5-color [green, violet, 756, 968, 889]	0.30 km	-2, 225	samples triple band, cyclodial band, plains terminator
	10 full	0.30 km	14, 225	coverage, Mannann'an crater high resolution
	7 full	0 22 km	0, 237	morphology of unexplored terrain
		0.03 km	25, 85	
E12	6-color [green, red, violet, 756, 968, 889]	1 4 km	-90, -90	global color
	1 full	0.180 km	-48, 299	fretted plateau
	4-color [green, violet, 756, 968]	0.170 km	11, 272	dark lineaments – color
	3-color [green, violet, 968]	0.125 km	-25, 271	Pwyll – color
	5 full	0.009 km	9, 274.4	high-resolution Chaos
	1 full	0.006 km	-13, 235	high-resolution mottled terrain
	8 full	0.012 km	-13, 235	high-resolution mottled terrain
	18 full	0.013 km	-16.4, 197	high-resolution – "wedges" terrain
	18 full	0.026 km	-17, 197	high-resolution – "wedges" terrain
	4 full	0.050 km		
E14	4 400 lines [green, red, violet, 968]	0.080 km	3, 240	4 color and high-resolution Mannann'an crater
	5 full	0 020 km		
	6 full	0.020 km	-2, 226	high phase, high-resolution dark material

Table 1. (continued)

Orbit	Frames (Full and Partial)	Resolution (per Pixel)	Center Coordinates	Notes
	4 400 lines [green]	0.040 km	24, 228	high phase photometry
	4 400 lines [green, red, violet, 968]	0.060 km	-2, 226	4 color high-resolution dark material
	8 400 lines	0.070 km	21, 213	high-resolution triple band structure
	9 full	0.170 km	35, 144	moderate-resolution coverage of Tyre multi-ring structure
	7 full	0.230 km	-27, 180	moderate-resolution anti-Jovian equatorial region, pull apart structures
	1 511 lines	0.230 m		
	2 240 lines			
	18 full (5 green, red, violet, 968) (3 768)	1.4 km	0, 195	4 color global color
E15	9 full	0.230 km	38, 222	regional mapping of trailing hemipshere
	3 partial [green, violet, 968]	0.210 km	28, 162	intermediate phase photometry
	3 full [green, violet, 968]	0.110 km	1, 180	color and stereo of Cilix crater, stratigraphy of crater material units
	16 400 lines	0.065 km		
	3 full	0.028 km	31, 142	high-resolution stereo of rough terrain SE of Tyre
	3 full	0.033 km		
	16 full	0.230 km	37, 89	regional mapping of leading hemisphere, global distribution of units
E17	1 full	4 km	-1, 162	global shape, leading anti-Jovian hemisphere
	19 full	0.220 km	-20, 210	regional mapping, trailing anti-Jovian hemisphere
	9 full	0.230 km	-20, 210	near terminator regional mapping
	5 400 lines	0.200 km	-20, 210	regional context, Agenor Linea
	4-color [violet, 756, 889, 968]	0.180 km	-20, 210	Agenor color
	5-color [green, violet, 756, 889, 968]	0.190 km	-42, 187	wedges color
	2 full	0.050 km	-29, 218	Chaos/plains boundary
	10 full	0.050 km	-44, 218	high-resolution Agenor Linea
	3 full	0.044 km	-48, 172	high-resolution Thrace Macula
	2 full	0.040 km	-53, 177	high-resolution Libya Linea
	9 full	0.040 km	-65, 195	high-resolution strike-slip fault in Astypalaea Linea
	1 full	0.040 km	-81, 197	high-resolution Rhiannon impact crater
	4 full	0.040 km	-66, 161	high-resolution Thynia Linea
	5 full	0.040 km	-80, 128	high-resolution south polar terrain
	19 full	0.220 km	-33, 82	regional mapping, leading sub-Jovian hemisphere
E19	1 400 lines	0.879 km	0, 200	tegid impact crater
	2 full	0.216 km	12, 181	sample stratigraphy
	2 full	0.200 km	16, 222	regional mapping
	3 full	0.200 km	65, 222	sample northern latitudes
	8 full	0.168 km	65, 225	sample northern plains
	4 full	0.064 km	35, 225	sample Rhadamanthys Linea
	4-color [green, red, violet, 968]	0.104 km	-2, 225	sample very high phase color
	4-color [green, red, violet, 968]	0.090 km	14, 225	sample very high phase color
	4-color [green, red, violet, 968]	0.083 km	22, 225	sample very high phase color of specular point
	30 full	0.072 km		limb scan plume search

disrupted, while other dark areas do not correlate with disrupted zones but might be areas that have been mantled by non-ice material. Still other dark areas appear to be deposits which flooded low-lying areas, based on embayment relations. Taken together, all of these were simply mapped in low resolution as "mottled terrain" on the Voyager images.

Galileo data suggest that Europa's icy lithosphere is composed of five primary units: plains, chaos, band, ridge, and crater-related materials, along with related subunits [*Greeley et al.*, 1998; *Head et al.*, 1998; *Senske et al.*, 1998; *Prockter et al.*, 1999a; *Figueredo and Greeley*, this issue; *Kadel et al.*, this issue]. In the following sections each of the primary units and their subunits is described, along with their type localities, letter abbreviations, and color designations suggested for mapping (Tables 2 and 3). Within this framework, mappers are likely to recognize additional subunits.

2.1. Plains Material (p)

Plains material is the most extensive geologic unit on the surface of Europa. It is subdivided into (1) ridged plains material, (2) smooth plains material, and (3) undifferentiated plains material. Ridged and smooth plains materials display characteristics visible at regional and local scales which enable them to be mapped. At global scale, plains material is mapped as an "undifferentiated" plains unit.

2.1.1. Ridged plains material (pr).

2.1.1.1. Description: Ridged plains material is characterized by planar areas with multiple crosscutting ridges and troughs that have parallel, subparallel, and multiple orientations (Figure 1). Individual ridges vary widely in length, width, and state of preservation [*Sullivan et al.*, 1999]. Ridges have a typical spacing of 100 m or more and may be locally anastomosing or crosscutting. In some locations, ridges in this unit lie in belts up to ~4 km wide with individual ridges spaced 200-400 m apart [*Sullivan et al.*, 1999]. Less organized sets of ridges are more randomly arranged and are typically composed of short ridge segments which have multiple orientations [*Greeley et al.*, 1998; *Patel et al.*, 1999]. Some ridges appear as single crests on global to regional resolutions and can be resolved into doublet or complex ridges on high-resolution images. In local areas (covering ~80 km^2 or less), ridged plains are subdued and slightly brighter than the surrounding terrain, and the ridges have little topographic relief. Ridged plains material may be interrupted locally with pits and domes. Contacts between ridged plains material and other units are usually sharp owing to topographic or albedo differences between the units. The fractured plains subunit described previously by *Lucchitta and Soderblom* [1982] is seen in both regional- and local-resolution Galileo images to consist of numerous ridges and troughs rather than fractures and is included in the ridged plains material. In some areas, ridged plains material has a subdued appearance in which the individual ridges have little relief.

2.1.1.2. Interpretation: The multiple ridges which make up this unit display a variety of sizes, orientations, and crosscutting relationships, suggesting that they formed by multiple episodes of ridge building [*Geissler et al.*, 1998a; *Patel et al.*, 1999; *Sullivan et al.*, 1999; *Figueredo and Greeley*, this issue]; alternatively,

Table 1. (continued)

Orbit	Frames (Full and Partial)	Resolution (per Pixel)	Center Coordinates	Notes
C20	2 partial	11.5 km	0, 58	eclipse observation; search for airglow
I25	3 full	0.090 km	90, 50	north polar region
	1 full	0.230 km	43, 354	dark bands
	1 partial	0.235 km	5, 330	near term imaging of E4 flows
	12 full	0 930 km	1.5, 20	mapping unexplored hemisphere
E26	2 full	0.011 km	-17, 350	ridges (nadir view)
	3 full, 1 partial	0.046 km	-17, 331	Callanish transsect
	3 full	0.107 km	6, 320	E4 flow features

Table 2. Type Localities of Map Units and Structures on Europa, With Relevant Galileo Image Data

Material Unit	Type Location (Latitude, Longitude)	Observation Name	Image (sClock Number)	Resolution (per Pixel)
	Map Units: Regional Resolution (hundreds of m/pixel)			
Plains material				
Ridged	27°, 218°W	E15REGMAP01	s0449961878	227 m
Smooth	16.6°, 278°W	E6DRKLIN01	s0383713701	180 m
Chaos material				
Platy	9°, 273°W	E6DRKLIN01	s0383713726	277 m
Knobby	-17°, 228°W	E17REGMAP01	s0466664613	173 m
Band material	-5.5°, 231°W	E11REGMAP01	s0420619252	262 m
Crater material				
c3 (Pwyll)	-26°, 274°W	E6PWYLL	s0383715504	308 m
c2 (Math)	-26°, 180°W	E14WEDGES	s0440955226	230 m
c1 (Tyre)	34°, 144°W	E14TYRE	s0440953640	170 m
	Map Units: Local Resolution (tens of m/pixel)			
Plains material				
Ridged	12°, 27°W	E6BRTPLN01	s0383718639	15 m
Smooth	5.7°, 326°W	E4DRKMAT02	s0374685452	25 m
Chaos material				
Platy	9°, 274°W	E6BRTPLN01	s0383717513	63 m
Knobby	36°, 86°W	E11MORPHY	s0420626739	34 m
Band material	35°, 87°W	E11MORPHY	s0420626752	34 m
Ridge material				
Double ridges	15°, 273°W	E6BRTPLN02	s0383718613	21 m
Complex ridges	6°, 326°W	E4HIRES	s0374685452	27 m
Crater material	-16.5°, 197°W	E12WEDGES	s0426273813	89 m
	Structure: Global Resolution (km/pixel)			
Ridge	53°, 178°W	G1GLOBAL	s0349875100	1.8 km
Strike-slip fault	-24°, 177°W	E14WEDGES	s0440984926	1.6 km
Lineament	44°, 239°W	G1GLOBAL	s0349875200	1.7 km
Depression	-26°, 168°W	E14GLOBAL	s0440984926	1.4 km
Dome	-48°, 160°W	E14GLOBAL	s0440984852	1.4 km
Crater rim	34°, 144°W	E14TYRE	s0440953640	degraded to 1 km
	Structure: Regional Resolution (hundreds of m/pixel)			
Ridge	-18°, 170°W	E14WEDGES	s0440955200	214 m
Trough	-34°, 174°W	E14WEDGES	s0440955265	309 m
Strike-slip fault	-26°, 171°W	E14WEDGES	s0440955239	260 m
Lineament	-16°, 196°W	E12WEDGES	s0426273800	133 m
Scarp	32°, 76°W	E15REGMAP02	s0449974339	254 m
Depression	33°, 226°W	E15REGMAP01	s0449961826	240 m
Dome	15°, 269°W	E6DRKLIN01	s0383713739	206 m
Crater rim	-26°, 274°W	E6PWYLL	s0383715504	308 m
	Structure: Local Resolution (tens of m/pixel)			
Ridge	14.7°, 274°W	E6BRTPLNS02	s0383718652	25 m
Trough	5.5°, 325°W	E4HIRES	s0374685139	36 m
Strike-slip fault	15.7°, 274°W	E6BRTPLNS	s0383718639	21 m
Lineament	-44°, 218°W	E17AGENORw	s0466669552	50 m
Scarp	-1°, 224°W	E14DRKSPT01	s0440948839	28 m
Depression	35°, 226°W	E19RHADAM01	s0484888726	79 m
Dome	8.7°, 275°W	E6DRKLIN01	s0383717500	64 m
Crater rim	-16.5°, 197°W	E12WEDGES	s0426273813	89 m

Table 3. Symbols Color Scheme Suggested for Geologic Mapping of Europa

Symbol	Map Unit	RGB Value
ps	smooth plains material	0, 38, 255 (dark blue)
pr	ridged plains material	140, 237, 255 (light blue)
pu	undifferentiated plains material	0, 149, 255 (medium blue)
chp	platy chaos material	79, 200, 66 (light green)
chk	knobby chaos material	0, 133, 0 (dark green)
b	band material (undifferentiated)	153, 51, 102 (dark purple)
r	ridge material (undifferentiated)	204, 153, 51 (orange-brown)
c	crater material (undifferentiated)	255, 255, 0 (yellow)
cs	smooth central unit	255, 255, 0 (yellow)
ci	inner rough unit	255, 255, 0 (yellow hatched)
cm	annular massif unit	205, 205, 100 (yellow brown)
ce	continuous ejecta unit	205, 205, 100 (yellow brown hatched)

Standard RGB (red, green, blue) values are identified for use in computer drafting software.

ridge building could be a continuous process. Several models have been proposed for the development of the ridges that form this unit (see section 2.4), including the accumulation of debris from repeated opening and closing of fractures [*Greenberg et al.*, 1998], cryovolcanic activity [*Kadel et al.*, 1998; *Fagents et al.*, 2000], and linear diapirism [*Head et al.*, 1999a]. Emplacement of ridged plains material appears to represent a style of tectonic resurfacing [*Head et al.*, 1997], as discussed in section 1.

Crosscutting relations in the areas seen in Galileo data show that ridged plains material includes the oldest recognizable units on Europa [e.g., *Greeley et al.*, 1998; *Head et al.*, 1999a; *Senske et al.*, 1998], but whether this style of surface formation was primarily contemporaneous with the formation of the other major units [*Greenberg et al.*, 1998] or was largely restricted to Europa's early (visible) history with a later transition to the other styles [*Head et al.*, 1999b; *Pappalardo et al.*, 1999; *Kadel et al.*, this issue] is not resolved. Nonetheless, most (but not all) ridged plains material appears to predate other units stratigraphically. The local occurrences of subdued ridged plains material is interpreted to represent areas that have been degraded, perhaps by viscous relaxation of the icy crust enhanced by local heating.

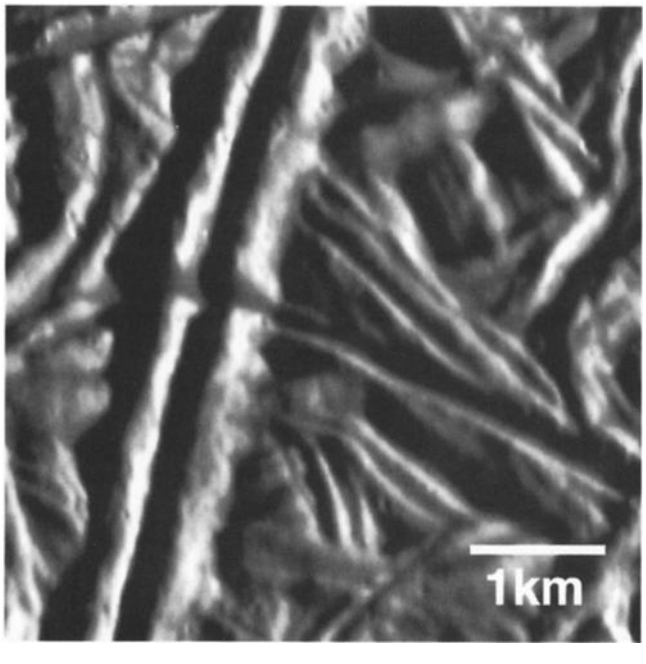

Figure 1. High-resolution (15 m/pixel) image of ridged plains material (Galileo frame s0383715504).

2.1.2. Smooth plains material (ps).

2.1.2.1. Description: This plains unit has a generally smooth surface with little or no visible texture and a lower albedo relative to the plains within which it occurs. Smooth plains material tends to embay, subdue, and/or overprint preexisting features (Figure 2), but contacts are usually distinct owing to the albedo contrast with adjacent units. Most smooth plains material is of limited areal extent and occurs in circular to irregularly shaped regions, suggesting that its emplacement was topographically controlled [*Greeley et al.*, 1998].

2.1.2.2. Interpretation: Smooth plains material is interpreted to result from (1) cryovolcanic emplacement of low-viscosity material onto the surface by effusion or cryoclastic deposition [*Greeley*,1997; *Fagents et al.*, 1998; *Wilson and Head*, 1999], (2) melting and recrystallization of surface materials due to a local near-surface heat source [*Pappalardo et al.*, 1998; *Head and Pappalardo*, 1999], or (3) some combination of these processes [*Greeley et al.*, 1998].

2.1.3. Undifferentiated plains material [pu].

2.1.3.1. Description: At global scales, plains material is mapped as undifferentiated (Figure 3) because features such as small ridges and ridge sets cannot be detected. Under high phase angle illumination, undifferentiated plains material has an overall smooth texture but locally contains irregular pits ranging in size from a few kilometers to ~100 km across [*Chapman et al.*, 1997; *Williams et al.*, 1999] and irregularly shaped isolated massifs that are a few kilometers across and usually <1 km high [*Greeley et al.*, 1998]. At visible wavelengths, contacts between undifferentiated plains materials and other units are less distinct at global resolutions, unless the units have significantly different albedos.

Undifferentiated plains material contains bright and dark subunits at infrared wavelengths [*Belton et al.*, 1996; *Geissler et*

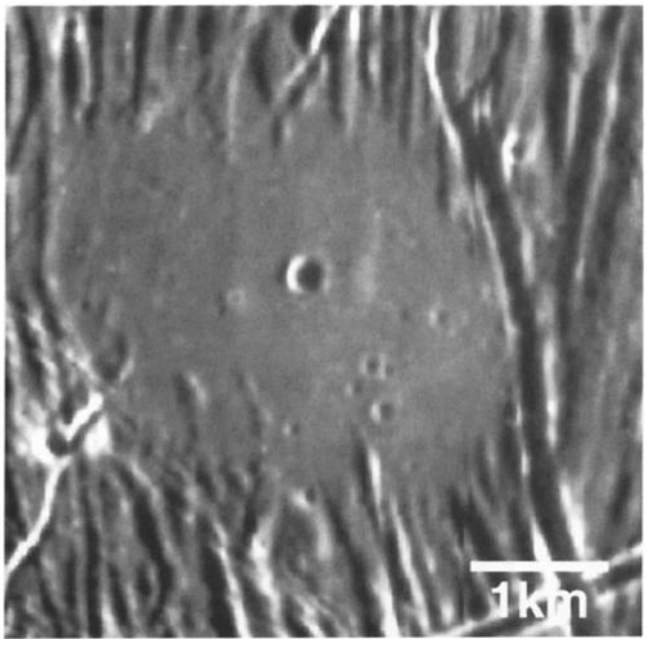

Figure 2. High-resolution (25 m/pixel) images of smooth plains material (Galileo frame s0374685452).

al., 1998a; *Helfenstein et al.*, 1998], which can only be observed in images taken at low phase angles. However, Galileo coverage is limited at these wavelengths, and consistent mapping of large areas is difficult. Undifferentiated plains material commonly contains bright and dark linear to curvilinear zones [*Smith et al.*, 1979a, b; *Lucchitta and Soderblom*, 1982; *Greeley et al.*, 1998] and is crosscut by continuous lineaments hundreds of kilometers long [*Smith et al.*, 1979a, b; *Belton et al.*, 1996; *Geissler et al.*, 1998a].

2.1.3.2. Interpretation: Undifferentiated plains material probably consists of ridged and smooth plains materials, as well as other units not visible at global scales. Consequently, this unit can span a wide range of geologic ages. Undifferentiated plains material observed in solid-state imaging (SSI) color data as being bright or dark in the near infrared is thought to represent differences in ice grain size [*Belton et al.*, 1996; *Geissler et al.*, 1998a].

2.2. Chaos Material (ch)

Chaos material is characterized by terrain that is disrupted into plates of icy crust of different sizes, set in a hummocky matrix which is generally at a lower elevation. Most chaos material appears to form at the expense of preexisting units [*Carr et al.*, 1998; *Greeley et al.*, 1998] and is among the youngest material found on Europa [*Spaun et al.*, 1998; *Prockter et al.*, 1999a; *Kadel et al.*, this issue]. However, some chaos material is cut by narrow lineaments and craters [*Greenberg et al.*, 1999; *Figueredo and Greeley*, this issue]. The contacts of chaos units with other units can be sharp or gradational. Typically, the contact is a pronounced scarp representing the breakup of the surrounding plains. However, the contact can also consist of a series of fractures grading into the surrounding, unaltered terrain. Galileo multispectral data show that most chaos areas are associated with the emplacement or formation of dark reddish material on Europa's surface. At regional and high resolution, two subunits of chaos material are recognized: knobby chaos material and platy chaos material, the latter being the more common of the two.

2.2.1. Platy chaos material (chp).

2.2.1.1. Description: This subunit of chaos material is composed of slabs or plates of preexisting material ranging in size from a few kilometers to tens of kilometers across and surrounded by a rugged matrix (Figures 4 and 5). The surfaces of the individual plates preserve surface features, such as ridges, of the terrain from which the plates were derived. The smallest plates on which such preserved features can be recognized are ~ 2 km across [*Carr et al.*, 1998]. In many cases the plates appear to have been rotated or moved from their original position. Like pieces of a jigsaw puzzle, many of the plates can be shifted or reassembled into their original position. Most of the plates appear to be at about the same elevation as the surrounding plains, although some are higher and others are lower. Although topographic data are limited, elevations derived from shadow measurements show that the relief from the upper surface of the plates to the matrix containing the plates ranges from about 10 to 100 m [*Giese et al.*, 1999b].

The matrix is composed of rugged hummocky terrain with individual hillocks ranging in size from a few hundred to a thousand meters across. There is no apparent orientation of the hillocks or other order to the hummocky texture [*Carr et al.*, 1998; *Spaun et al.*, 1998].

2.2.1.2. Interpretation: Several ideas have been proposed to explain the formation of chaos terrains and the resulting materials. Most of the hypotheses involve material rising toward the surface, driven by either heat or differences in material density [e.g., *Collins et al.*, 2000]. This material either breaks through to the surface or disrupts the surface, fracturing the ice lithosphere into plates and moving them into new positions [*Williams and Greeley*, 1998]. *Spaun et al.* [1998] have shown that in the Conamara Chaos region, ~59% of the original background terrain has been either destroyed, modified, or

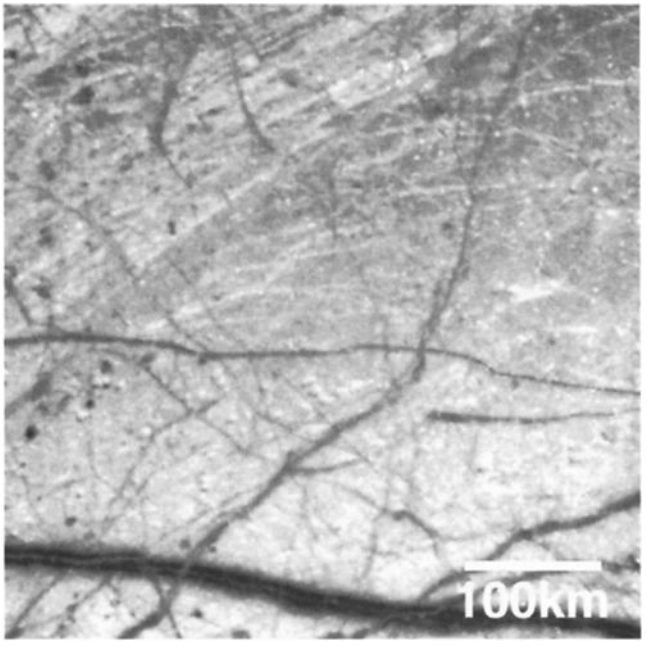

Figure 3. Global-resolution clear filter image of undifferentiated plains material (Galileo frame s0349875100).

replaced as matrix material. All current models [*Greenberg et al.*, 1998, 1999; *Pappalardo et al.*, 1998; *Spaun et al.*, 1998; *Head and Pappalardo*, 1999] suggest that chaos terrain formed directly above a heat source. However, there is some debate as to the nature of the heat source. *Greenberg et al.* [1999] believe that the large fragments observed in platy chaos represent blocks that are analogous to buoyant icebergs set within denser, low-viscosity matrix material composed of water or a water-ice slurry. *Pappalardo et al.* [1998], *Spaun et al.* [1998], and *Head and Pappalardo* [1999] all suggest that warm ice rises toward the surface as a solid-state convection cell or as a diapir which disrupts the rigid lithosphere. Within the platy chaos material the individual fragments are interpreted as remnants of lithosphere which were essentially unaffected by the thermal processes that formed the matrix material [*Spaun et al.*, 1998]. Small blocks and hillocks within this matrix could represent remnants of larger fragments that have undergone considerable disruption by thermal or mass-wasting processes.

2.2.2. Knobby chaos material (chk).

2.2.2.1. Description: This subunit of chaos material is characterized by irregularly shaped knobs that stand above the surrounding matrix; plates of preserved plains material are generally lacking (Figure 6). Individual knobs are as large as 3 km across and stand tens of meters to a few hundred meters above the matrix. In some cases, areas of knobby chaos are observed to stand as high as 150 m above the surrounding units (e.g., "the mitten" [*Figueredo et al.*, 1998, 2000]) and are collectively referred to as "raised chaos."

2.2.2.2. Interpretation: Knobby chaos material may be analogous to the matrix in platy chaos material, and thus it might represent material that has been thermally altered and disaggregated to such an extent that polygonal plates are no longer recognizable [*Head et al.*, 1999c]. In some areas, however, the morphology of knobby chaos material suggests that it might have been areas of platy chaos material that were subsequently disrupted [*Figueredo et al.*, 1998]. In addition, some high-standing blocks and patches of hummocky terrain found in some ridged plains units might represent ancient chaos terrain that has been overprinted by ridged plains [*Greenberg et al.*, 1999]. The positive relief of raised chaos has been attributed to expansion following the refreezing of local melts [*Greenberg et al.*, 1999] or the cryovolcanic/diapiric emplacement of subsurface materials [*Collins et al.*, 2000; *Figueredo et al.*, 2000].

Consensus on the composition of Europa's dark reddish material is yet to emerge, with two classes of candidate materials under investigation. These are (1) hydrated salt minerals, possibly

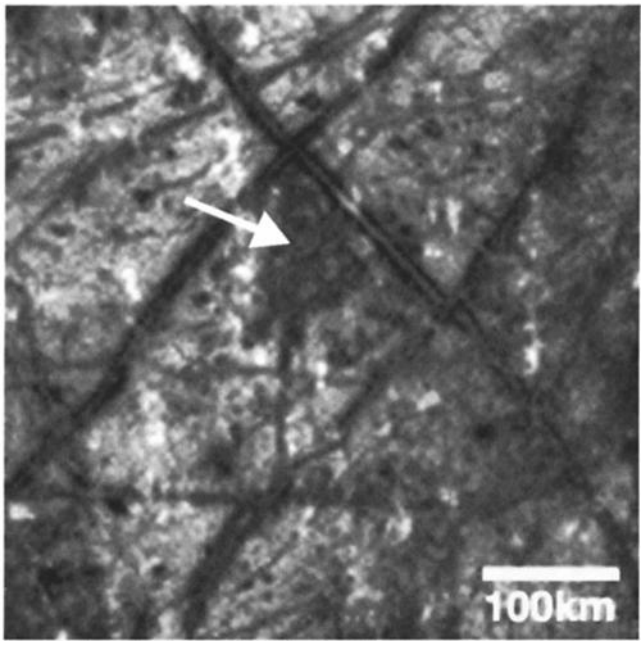

Figure 4. Global-resolution image of a region containing chaos material (arrow below X-shaped bands; Galileo frame s0360063913).

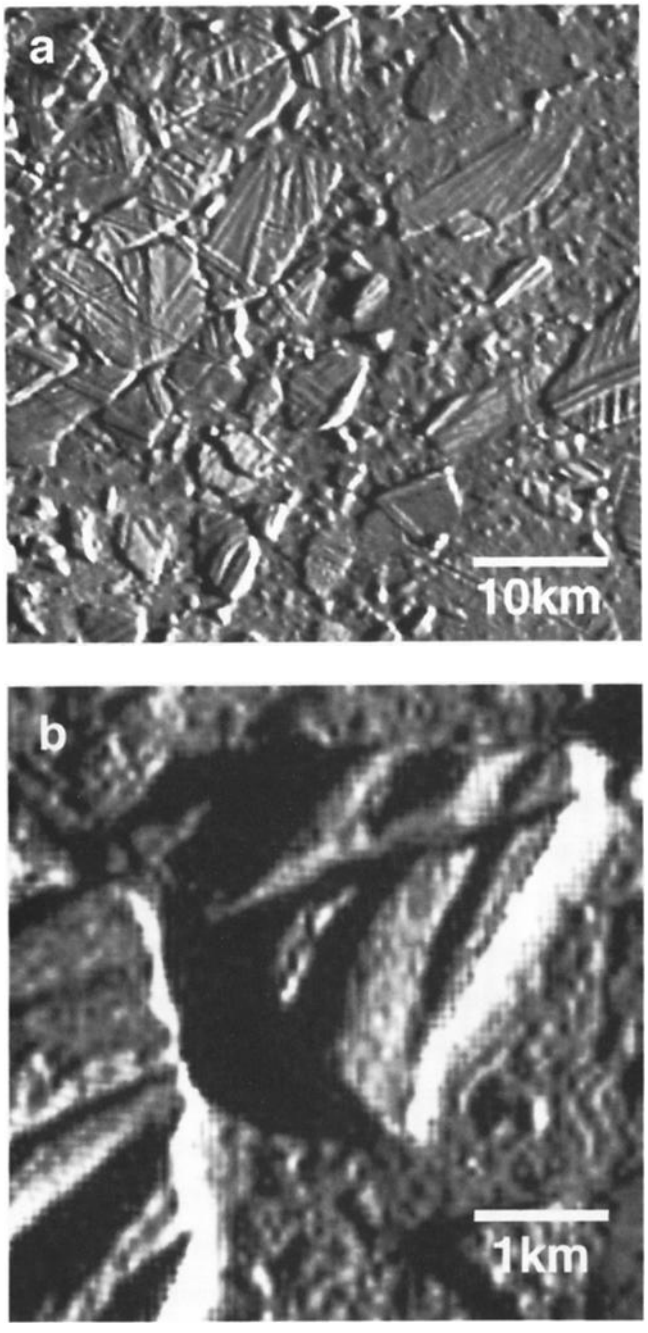

Figure 5. (a) Moderate-resolution (227 m/pixel) image of platy chaos material (Galileo frame s0383713726). (b) High-resolution (63 m/pixel) image of platy chaos material (Galileo frame s0383717513).

representing evaporites of subsurface ocean brines [*McCord et al.*, 1998, 1999], and (2) hydrated sulfuric acid, generated during one phase of radiolytic sulfur cycle [*Carlson et al.*, 1999]. We note that the former are not colored materials and would require an admixed coloring contaminant, whereas sulfur chains serve to color the latter.

2.3. Band Material (b)

2.3.1. Description: The term "band" is applied to linear zones distinguished by their contrast in albedo or surface texture compared with the surrounding terrain; as such, their contact is usually well defined. As originally applied to the analysis of Voyager images, band material included triple bands, gray bands, bright bands, and wedge-shaped bands [*Smith et al.*, 1979b; *Lucchitta and Soderblom*, 1982]. In some Voyager images the central bright stripes of triple bands were recognized as ridges [*Malin and Pieri*, 1986]. Galileo data confirm that triple bands are doublet ridges flanked by darker material [*Belton et al.* 1996], and we include these features in section 2.4.

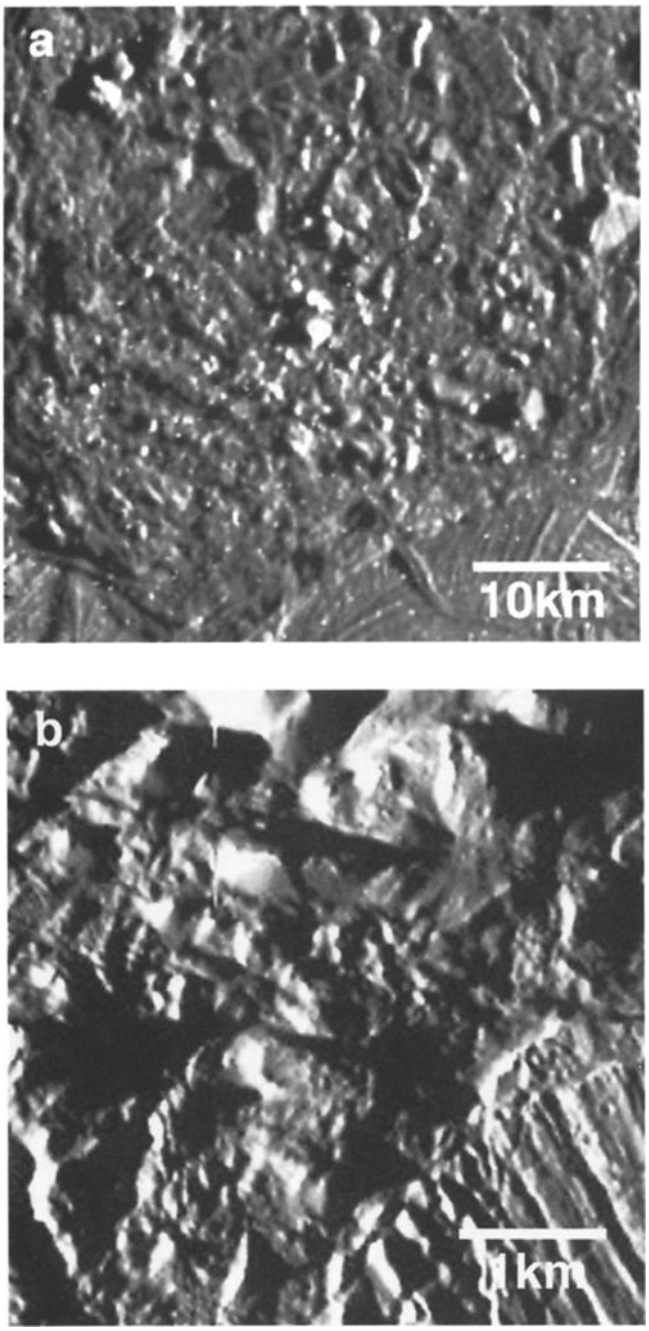

Figure 6. (a) Moderate-resolution (173 m/pixel) image of knobby chaos material (Galileo frame s0466664613). (b) High-resolution (34 m/pixel) image of knobby chaos material (Galileo frame s0420626739).

At global resolutions, band material is seen to form linear, curvilinear, cuspate, or wedge-shaped features with sharp, parallel-to-subparallel margins (Figure 7). In some cases, exterior lineaments and other surrounding features that terminate at band margins can be reconstructed by moving opposing band margins together [*Schenk and McKinnon*, 1989; *Golombek and Banerdt*, 1990; *Pappalardo and Sullivan*, 1996; *Sullivan et al.*, 1998]. Some bands also show strike-slip displacements [*Schenk and McKinnon*, 1989; *Tufts et al.*, 1999; *Prockter et al.*, 2000]. When viewed away from the terminator, band interiors commonly are darker than surrounding plains. Near the terminator, where material brightness contrasts are difficult to detect (if present), some band material is distinguished from surrounding terrain by different textures, e.g., as a narrow, sharply bounded polygonal area with distinctly fewer superposed ridges than surrounding terrain. There is a wide range of albedos among bands. In most areas studied, younger bands seen at global resolution have lower albedos than the older bands they crosscut [*Sullivan et al.*, 1998; *Tufts et al.*, 1999; *Prockter et al.*, 1999a]; Agenor Linea is an important exception [*Prockter et al.*, 2000].

At regional resolution the characteristics noted above are more easily distinguished. In many places, band margins consist of bounding ramps. In some instances the transition from the surrounding terrain to the band interior is marked by single or doublet ridges along margins of the band. Band interiors appear to stand slightly higher than surrounding terrain, at least along band margins where illumination and resolution permit comparison. More rigorous stereoscopic analysis in one case shows that band material stands at least 100 m above the surrounding plains [*Giese et al.*, 1999b]. In other areas, band margins show little relief compared with surrounding terrain, and the transition between the band interior and exterior is abrupt and without conspicuous structure or relief. At its simplest, band interior morphology is smooth and featureless at 200 m/pixel. When viewed at higher resolutions (Figure 8), many of these same "smooth" band interiors reveal subtle, small-scale surface roughness and flow-like patterns. A central trough or ridge may be prominent, and in these cases other interior ridges and troughs can be bilaterally symmetric about the central lineament. Additional lineations within band materials such as doublet ridges and secondary systems of alternating ridges and troughs add complexity to the morphology of bands.

2.3.2. Interpretation: The observation that opposing band margins commonly can be reconstructed by eliminating intervening band interior materials has indicated to many workers that bands form initially from fractures along which the lithosphere separated, the intervening gap filled with material derived from the subsurface [e.g., *Schenk and McKinnon*, 1989; *Golombek and Banerdt*, 1990; *Pappalardo and Sullivan*, 1996; *Sullivan et al.*, 1998; *Prockter et al.*, 1999b; *Greenberg et al.*, 1998]. The variety of band interior morphologies suggests that different mechanisms, or perhaps the same fundamental mechanism operating at different rates [*Prockter et al.*, 1999b;

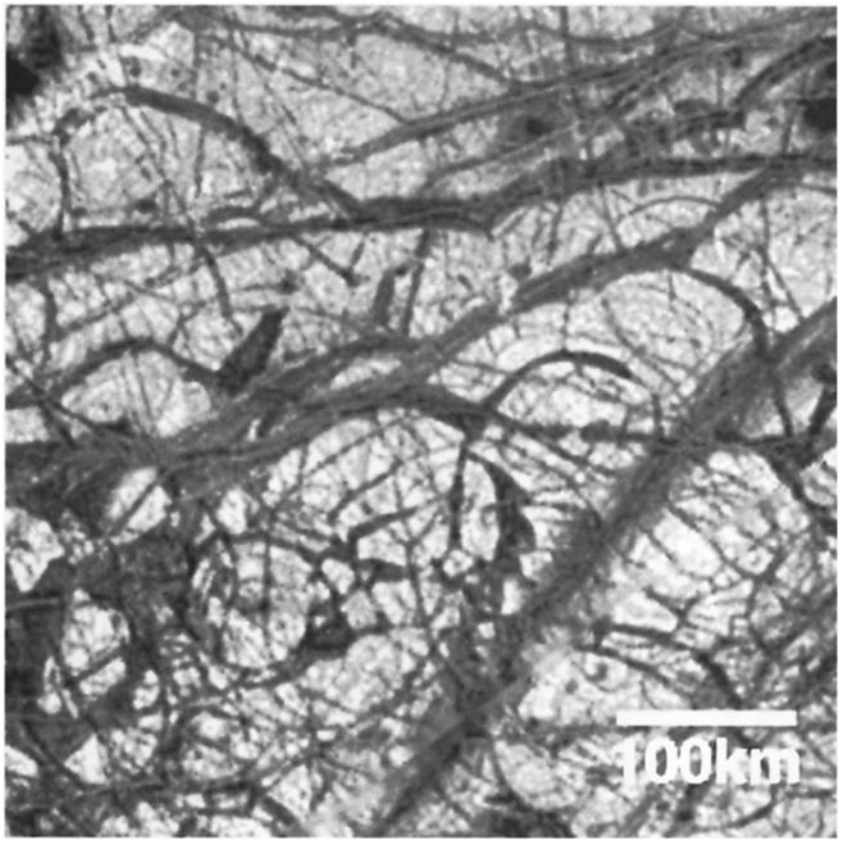

Figure 7. Global-resolution (1.7 km/pixel) image of band material in the anti-Jovian hemisphere (Galileo image s0349875126).

Tufts et al., 2000], can develop a band from an initial fracture as opposing plate margins spread apart. It has been suggested that bands represent the last stage in an evolutionary sequence in which doublet and complex ridges (described below) are intermediate steps in the process [*Pappalardo et al.*, 1998; *Geissler et al.*, 1998a].

Within many bands the bilateral symmetry of features is consistent with repeated emplacement of material primarily at the band center, with older band material moving to each side to make way for newer material rising from below as plates of preexisting material continued to move farther apart [*Sullivan et al.*, 1998]. Episodic emplacement of icy material from the near-subsurface along a spreading axis is consistent with internal morphologies parallel to the margins of the bands [*Sullivan et al.*, 1998; *Prockter et al.*, 1999b]. Other models consider that ridged bands formed by progressive building of ridges or ridge pairs [e.g., *Greenberg et al.*, 1998]. In these models the weight of a doublet ridge fractures the surrounding plains, and new ridges develop from the fractures along the margins. In bands where no ridge buildup is apparent, other mechanisms might have operated. This is evident in a few cases where sharp blocks were formed by normal faulting [*Prockter et al.*, 1999b; *Figueredo and Greeley*, this issue].

2.4. Ridge Material (r)

2.4.1. Description: Ridge materials form the dominant surface features on Europa. They form ridges which range in width from ~200 m to >4 km, can be short or can exceed 1000 km in length, and are as high as 200-350 m [*Kadel et al.*, 1998]. Ridges include features that are straight, curvilinear, or cycloidal (congruent curved segments joined at sharp cusps). Ridge material forms single ridges, doublet ridges (two ridges separated by a trough: Figure 9), or ridge complexes (Figure 10) consisting of more than two ridges. Ridge complexes can form anastomosing and discontinuous sets of ridges and include ridges and sets of ridges which "split" away from the main trend of the complex [*Figueredo and Greeley*, this issue]. The topographically high morphology of ridge material makes their contacts distinct with surrounding units.

The detection of various ridges is a function of image resolution and illumination. At global scales, many lineaments are seen to be ridges, especially when viewed near the terminator. Because they are too narrow on global- and regional-scale maps, these are typically mapped with structural symbols, rather than as material units (see section 3).

Triple bands were described on Voyager images as lineaments consisting of a bright stripe flanked on each side by dark bands [*Lucchitta and Soderblom*, 1982]. Galileo images show that most triple bands are doublet ridges (the bright part seen on Voyager images) flanked by dark, diffuse material which lacks a sharp outer margin [*Belton et al.*, 1996].

In high-resolution images the cross section of some ridges is seen to have steep outer flanks, rising to a flat-topped summit. The steep flanks of some ridges consist of mass-wasted material, apparently emplaced at its angle of repose (Figure 9). Stereoscopic images of other ridges reveal that the flanking terrain is elevated [*Giese et al.*, 1999a, b]. In other areas, ridges are flanked by depressions, some of which are marked by parallel fracturesolution

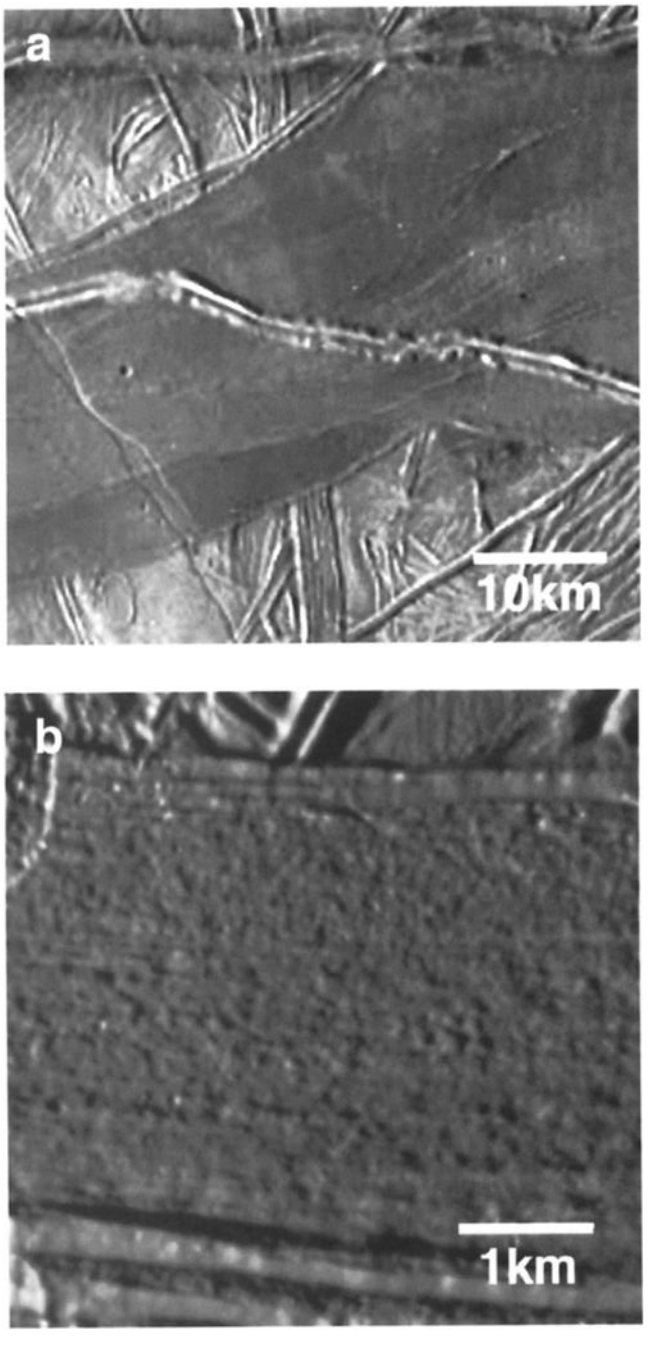

Figure 8. (a) Moderate-resolution (262 m/pixel) image of band material (Galileo frame s0420619252). (b) High-resolution (34 m/pixel) image of band material (Galileo frame s0420626752).

2.4.2. Interpretation: Several models have been proposed to explain ridge formation on Europa, including accumulation of fragmental debris from tectonic [*Greenberg et al.*, 1998] or cryovolcanic processes [*Kadel et al.*, 1998], upwarping owing to localized heating and linear diapirism [*Head et al.*, 1999a], incremental wedging [*Turtle et al.*, 1998], or compression of material localized by an initial fracture or set of fractures [*Sullivan et al.*, 1998]. Crosscutting relationships and orientations of some ridges suggest that the original fractures may be controlled by stresses resulting from tidal deformation [*Hoppa et al.*, 1999] and/or nonsynchronous rotation of the satellite [*Geissler et al.*, 1998b]. Evidence for all of these

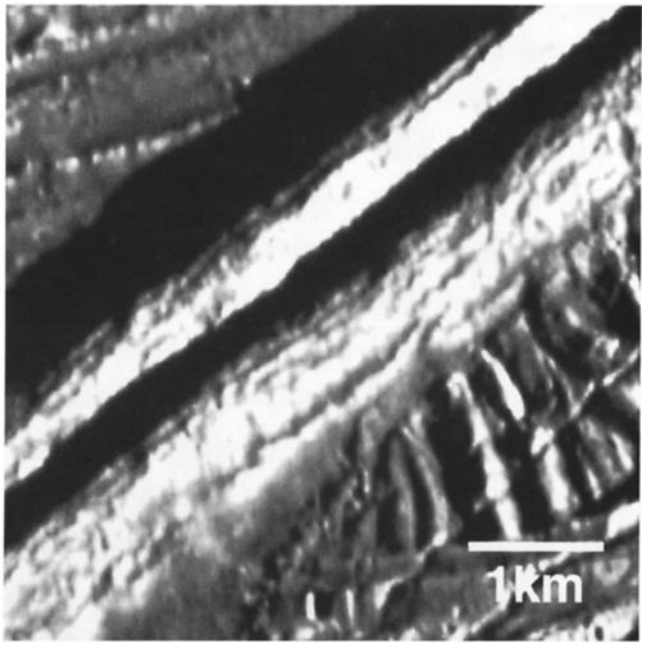

Figure 9. High-resolution (21 m/pixel) image of doublet ridge material (Galileo frame s0383718613).

hypotheses can be cited, and it is possible that ridges form by a combination of mechanisms.

2.5. Crater Material (c)

Crater material is classified stratigraphically as c1 (oldest craters), c2, and c3 (youngest craters). The c1 craters are recognized only as remnants of impact by the presence of concentric lineaments, central palimpsest-like terrain, and fields

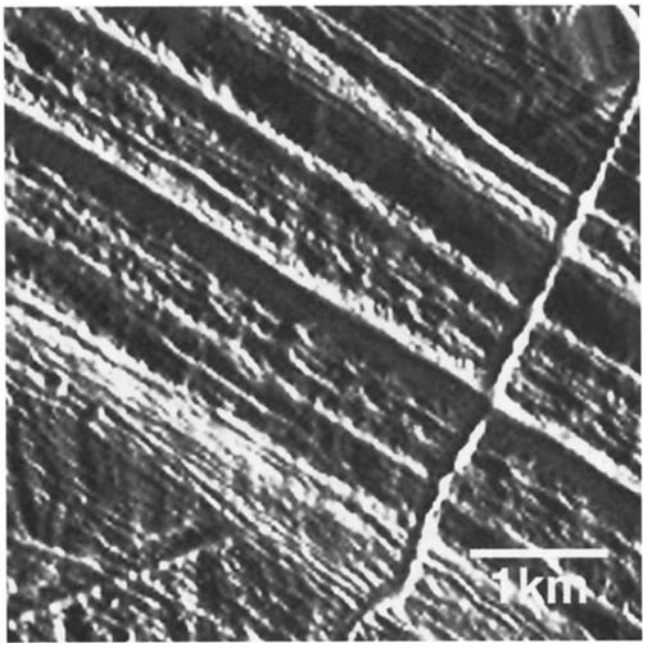

Figure 10. High-resolution (27 m/pixel) image of complex ridge material (Galileo frame s0374685452).

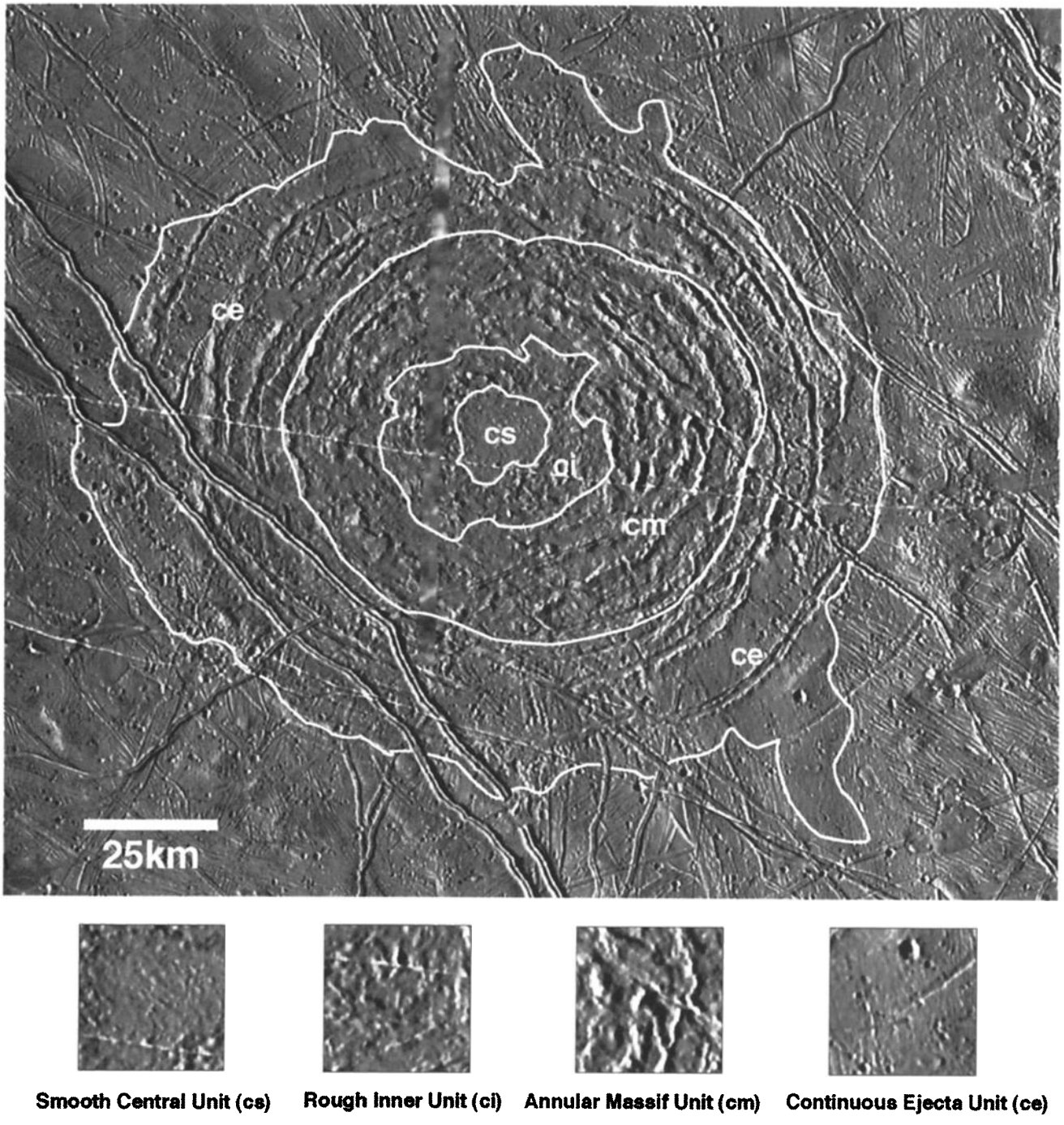

Fig. 11. Global-resolution image of the Tyre multiring impact structure, with the four units described in text.

of inferred secondary craters. The c2 craters have well-preserved crater rims and continuous ejecta deposits but lack ray systems. The c3 craters have relatively sharp rims and either bright or dark ejecta deposits, including well-defined rays. Although large impact craters are rare on Europa, Galileo images reveal two multiring impact structures larger than ~50 km in diameter (Tyre and Callanish, both of which are c1 craters) and several craters >15 km in diameter (Pwyll, a c3 crater). We have defined crater subunits on the basis of study of the Tyre (Figure 11) impact structure and the smaller craters Manan'an and Pwyll [*Moore et al.*, 1998].

2.5.1. Smooth Central Unit Description. In multiring impact structures the smooth central sub unit (cs) consists of smooth to slightly hummocky materials which tend to have a higher albedo and lower elevation than the surrounding terrain.

2.5.2. Interpretation: This material is considered to be frozen melt formed by the impact.

2.5.3. Inner Rough Unit Description: An inner rough sub unit (ci) is characterized by closely spaced kilometer-size equant to elongate hills with no clear organization.

2.5.4. Inner Rough Unit Interpretation: This material may include sections of collapsed crater wall and disrupted background plains. The position of the transient cavity rim is thought to lie within this region.

2.5.5. Annular Massif Unit Description: An annular massif sub unit (cm) includes arcuate elongate blocks arranged concentrically outside the periphery of the rough inner unit.

2.5.6. Annular Massif Unit Interpretation: The blocks could be remnants of preexisting terrain and structures deformed by the impact. This material is interpreted as icy lithosphere that was uplifted and fractured during impact. In some smaller craters, isolated angular massifs (interpreted to be uplifted target material) are found within the central crater floor unit.

2.5.7. Ejecta Unit Description: In craters of all sizes a smooth to finely -textured material (subunit ce) buries preimpact terrain.

2.5.8. Ejecta Unit Interpretation: The material is considered to be ejecta emplaced in a fluidized state, suggested by embayment relationships [*Moore et al.*, 1998]. Abundant small pits, some linked in chains and radial to the structure, are interpreted to be secondary impact craters [*Moore et al.*, 1998].

3. Structural Features and Landforms

Europa displays a complex surface history of tectonic disruption and a variety of landforms which are best shown on geological maps with symbols. Structures include ridges (where too small to be mapped as material units), troughs, strike-slip faults, and lineaments. Landforms and other features to be shown with symbols include scarps, depressions, domes, and crater rims. The means for mapping these features and their portrayal on geological maps follow the convention of *Wilhelms* [1972, 1990] with minor modification.

3.1. Ridges

The general nature of Europan ridges is described in section 2.4. Ridges should be mapped with structural symbols at global and regional scales by a line along the ridge axis, marked with outward pointing diamonds (Figure 12). Some ridges or bands contain multiple, subparallel linear features; inferred structural components can be mapped as lineaments, and this may include mapping representative examples of an inferred trend where too many features are present to map individually, following the approach used for Ganymede [*Wilhelms,* 1990].

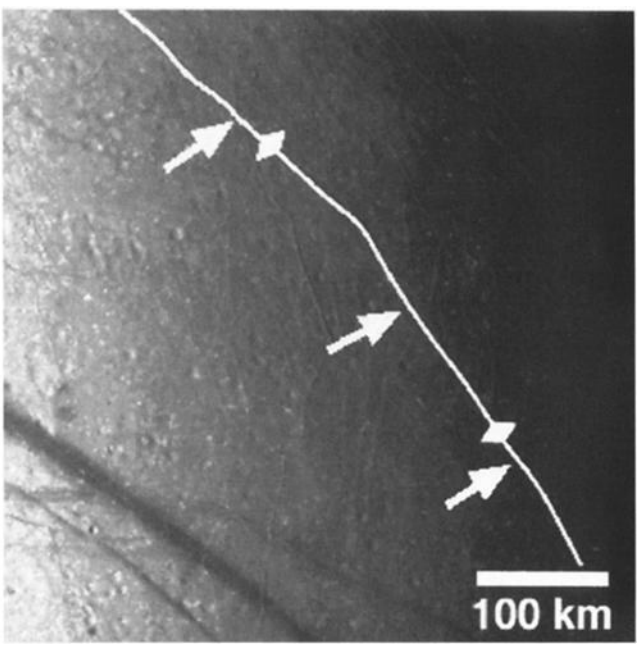

Figure 12. Structural symbol for mapping ridges at global resolution. The symbol is a line along the ridge axis with barbs which point away from the axis (Galileo frame s0349875100; 1.8 km/pixel resolution).

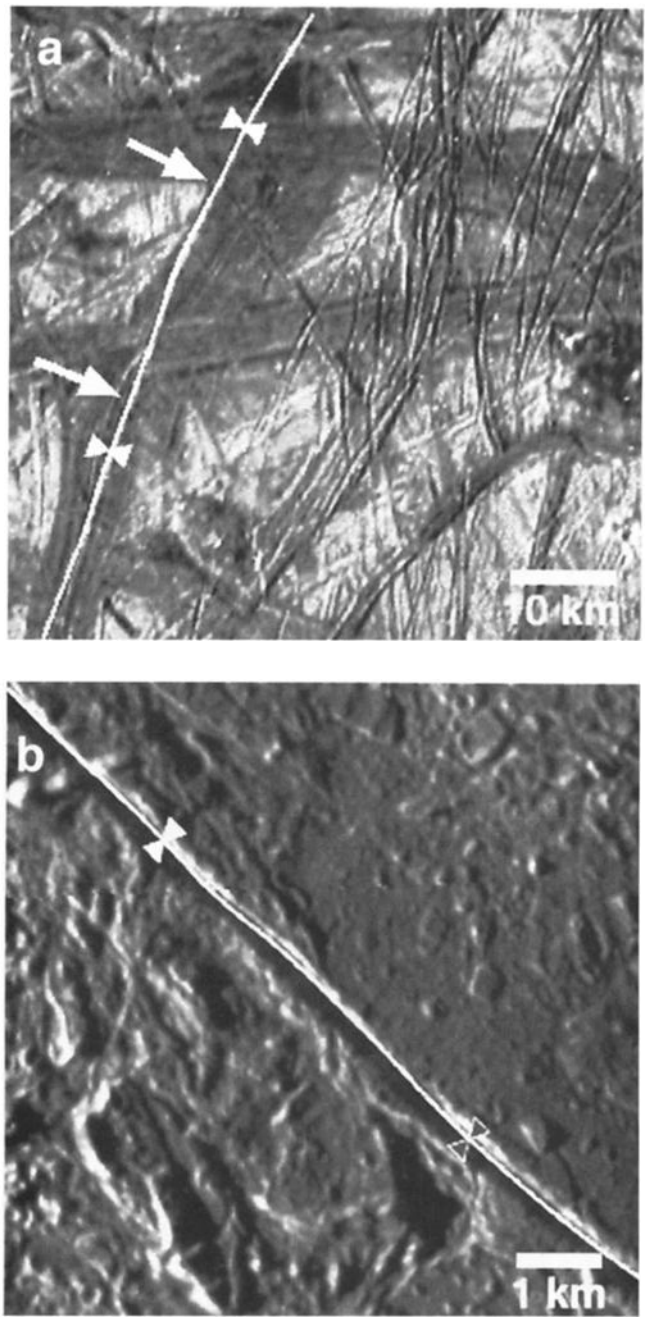

Figure 13. (a) Structural symbol for mapping troughs at regional resolution (Galileo frame s0440955265; 309 m/pixel resolution). (b) Structural symbol for mapping troughs is a line drawn in the middle of the trough floor with inward pointing barbs (Galileo frame s0374685139; 36 m/pixel resolution).

3.2. Troughs

Troughs are generally V- or U-shaped in cross section and often have slightly raised rims. Flat-floored and/or curvilinear

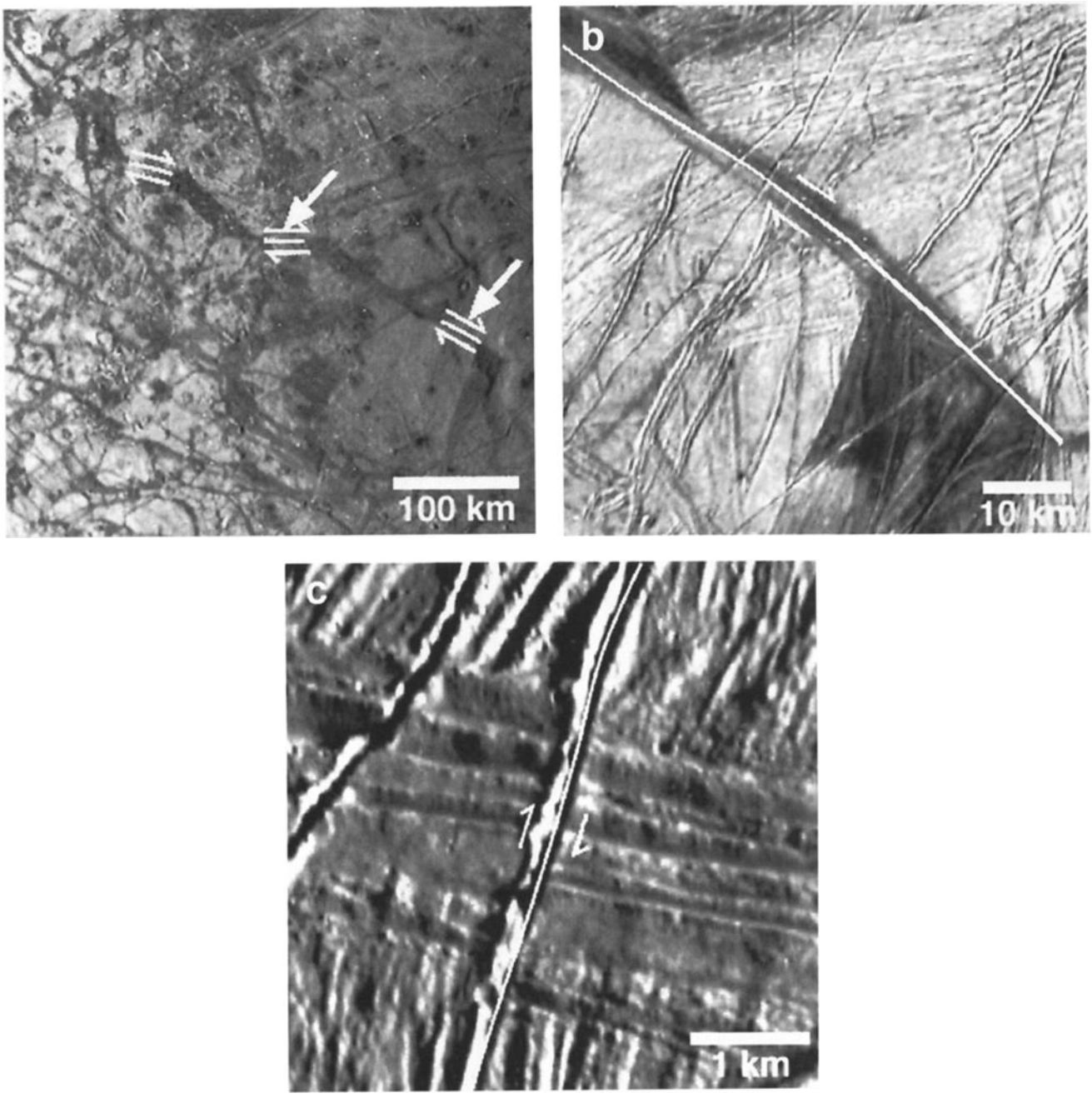

Figure 14. (a) Structural symbols for mapping strike-slip faults at global resolution (Galileo frame s0440984926; 1.6 km/pixel resolution). (b) Structural symbols for mapping strike-slip faults at regional resolution (Galileo frame s0440955239; 260 m/pixel resolution). (c) Structural symbols for mapping strike-slip faults at local resolution (Galileo frame s0383718639; 21 m/pixel resolution).

troughs occur less frequently. They can transect all terrain types. Because they are narrow, troughs are not generally recognized at global scales but appear as lineaments (section 3.4). Troughs are mapped with a line along the trough axis (Figure 13) and have solid inward-pointing arrowheads (a "bow tie" symbol). A flat-floored and/or curvilinear trough may be mapped with an alternate symbol, such as an open inward pointing arrowhead.

3.3. Strike-Slip Faults

Strike-slip faults are implied where lateral displacement of older features is inferred. Structural features along which lateral motion apparently occurred include ridges, troughs, lineaments, and scarps. A strike-slip fault is mapped with a line along which the faulting has occurred, with flanking half-arrows indicating the direction of relative motion (Figure 14).

3.4. Lineaments

Lineaments include a variety of narrow linear features that have ambiguous or no discernible relief and which cannot be sufficiently resolved for more exact descriptions. Examples include narrow albedo features seen at global resolution and low incidence angle, which might be revealed as doublet ridges or

rimless troughs at higher resolution and near-terminator illumination. At higher resolutions and higher incidence angles the term lineament is applied to linear textural features in bands (usually aligned parallel or subparallel to band margins), as well as single features that are indistinct or insufficiently resolved for more definitive identification. Lineaments are mapped with a dashed line along the feature (Figure 15); this may include mapping only representative examples of the structural trend.

3.5. Scarps

Scarps are sharp breaks in topography with slopes that are distinguished from ridges and troughs by their isolation (i.e., scarp slopes are not paired with another slope facing in the opposite direction). Scarps are distinguished from closed crater rims, depressions, and domes by being linear to curvilinear in planform. They generally are not recognized at global scales but appear as lineaments. A scarp is mapped with a line, generally along the base of the slope with hachures pointing in the downslope direction.

3.6. Depressions

Depressions are enclosed circular, elliptical, or irregularly shaped negative-relief features with tens to hundreds of meters of relief. They are most easily recognized under near-terminator lighting conditions. Some contain or are associated with low-albedo material. At regional and local scales some depressions are recognized to contain chaos or smooth plains material. A depression is mapped by a line that follows the outline of its upper slope and marked with downslope-directed hachuresolution

3.7. Domes

Domes are subcircular to elliptical positive-relief features tens to hundreds of meters high. They are most easily recognized under near-terminator lighting conditions. Some domes have the same albedo as the surrounding terrain. At regional and high resolution the surrounding background plains are commonly recognized to continue largely undisturbed on top of such domes [*Pappalardo*, 2000]. Other domes have distinctly different albedos from the background ridged plains, suggesting that they may consist of materials different than the surrounding terrain, in which case they could be mapped as material units [e.g., *Figueredo and Greeley*, this issue]. A dome is mapped with a line along its base and marked with outward pointing hachuresolution

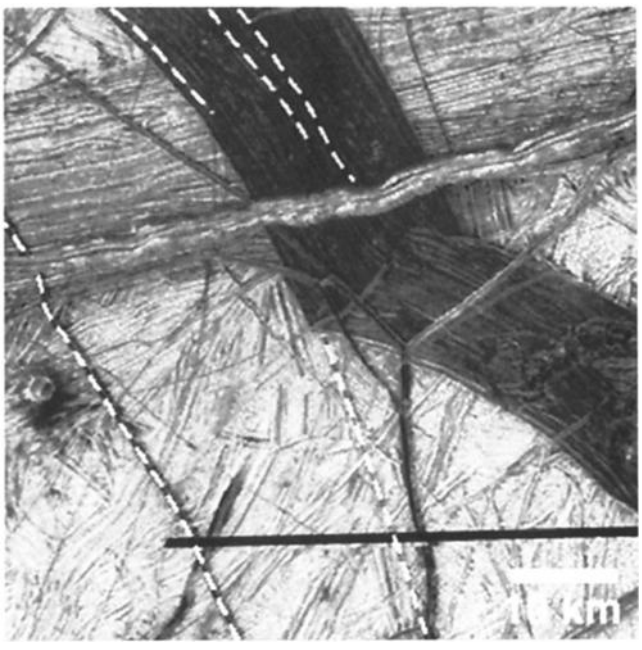

Figure 15. Structural symbol for mapping lineaments at regional resolution (Galileo frame s0426273800; 133 m/pixel resolution).

3.8. Crater Rims

Crater rims are circular structures, typically raised above surrounding terrain and enclosing a depression. The crater rim generally divides interior floor deposits from exterior deposits. Relatively large craters (larger than ~15 km) have complex morphologies, commonly showing a central peak or peak complex. At high resolution, small craters and pits are observed, with less apparent or negligible raised rims. Some small craters occur in clusters.

A crater rim is mapped with a closed circular curve along the rim crest and sets of paired inward pointing hachuresolution. Central peaks, where they occur within craters, are mapped by an ellipse with four radiating hachures for a large peak, or a plus sign for a small peak. Craters or pits too small to accommodate inward pointing twin hachure marks and/or with no discernable rim crest are mapped with a closed circular curve that outlines the rim. In all cases the line is dashed where the rim is uncertain.

4. Stratigraphy

Preliminary mapping [*Head et al.*, 1998; *Klemaszewski et al.*, 1999; *Senske et al.*, 1998; *Greenberg et al.*, 1999; *Prockter et al.*, 1999a; *Spaun et al.*, 1999; *Figueredo and Greeley*, this issue; *Kadel et al.*, this issue] and analyses conducted as part of this study suggest a stratigraphic sequence for Europa, as shown in Figure 16. The oldest recognizable unit is ridged plains material. It appears to form by tectonic processes, perhaps accompanied by local extrusion of material from the subsurface. The fracturing preceding in ridge formation most likely resulted from tidal flexing and nonsynchronous rotation of Europa's icy lithosphere.

Two models are suggested for the formation and evolution of ridged plains material. One model suggests that various ridges, bands, and ridged plains materials are part of a continuum, in which ridges evolve into complex ridges, then into bands, and then into ridged plains. A second model suggests that ridged plains material represents a fundamentally different process. Regardless of which model (or other models) might be correct, the correlation chart (Figure 16) shows most ridged plains being stratigraphically older than band material and individual ridges.

Most chaos terrain is stratigraphically younger than ridged plains. The two forms of chaos, knobby and platy, could reflect differences in styles or degrees of formation or differences in the properties of the material from which they form. All interpretations for the formation of chaos terrain included endogenic processes, such as diapiric intrusion of low-density materials which erupt onto the surface, heat-driven mantle upwellings, melting of the icy crust, and/or the extrusion of subsurface material in a style of local cryovolcanism. High-standing blocks of icy crust and knobby terrain found in some ridged plains areas suggest former chaos terrain that has been modified by ridged plains formation. If this interpretation is

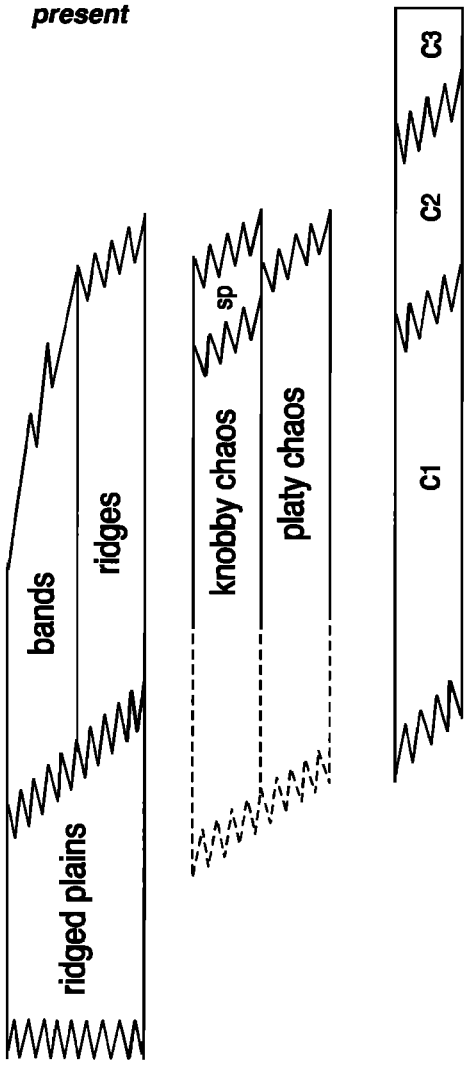

Figure 16. Preliminary correlation chart of Europan material units, as derived from mapping of available Galileo data. Younger units are shown above older units; "saw-tooth" lines indicate uncertain boundary ages; diagonal lines reflect transitional or overlapping boundaries. The chart incorporates the possibility of early (i.e., contemporaneous with ridge plains) formation of chaos terrain and local occurrence of some ridges after events of chaos formation. The relationship among ridged plains, bands, and ridges is unclear; ridged plains material could have formed by accumulation of numerous and closely spaced lineaments, or it may have resulted from a separate process.

correct, then the processes leading to chaos terrain formation have operated through much of the visible history of Europa.

Smooth plains materials are of limited extent in the areas imaged by Galileo. These dark areas appear to represent local flooding of the surface by fluid materials extruded from the subsurface, although, alternatively, they could also represent melt-through and/or partial melting about diapirs. Although some smooth plains are crosscut by banded materials, most smooth plains appear to be among the youngest materials on Europa.

The oldest impact craters recognized on Europa are classed as c1 craters. These craters include the Tyre and Callanish structures, which are low-relief and lack widespread bright ejecta deposits, although both do have fields of abundant secondary craters. Their lack of relief suggests impacts into a thin brittle icy lithosphere overlying a viscous or fluid substrate and/or degradation by viscous relaxation through time. The c2 craters constitute most of the craters > 10 km on Europa. A few are cut by ridges, bands, or small patches of chaos terrain. The youngest craters (c3) are found in most areas and are characterized by bright ejecta rays. Secondary craters from these impacts occur as clusters in many parts of Europa, including the matrix in chaos terrains [*Bierhaus et al.*, 1998].

The absolute timescale for Europa remains enigmatic. The fundamental problem is the extrapolation to the Jovian system from the crater counts that have been calibrated for Earth's Moon by radiometric dates based on lunar samples. As reviewed by *Neukum* [1997], *Zahnle et al.* [1998], and *Pappalardo et al.* [1999], such extrapolations are highly model dependent, and there are different approaches that can be used. A basic assumption in the Neukum model is that ages in the Jovian system can be derived by assuming that the largest and youngest basins seen on Ganymede are equivalent to the youngest basins on Earth's Moon and that subsequent dates in the Jovian system can be extrapolated from the flux derived for the Moon. A basic assumption in the *Zahnle et al.* [1998] model is that the currently observed bodies in the outer solar system can be used to extrapolate an impact flux backward through time to derive surface ages. In the *Neukum* [1997] model, Europa's surface is as old as ~ 3 Gyr, while in the *Zahnle et al.* [1998] model, the surface is ~ 50 Myr. Until some calibration is obtained for impact flux in the outer solar system, the uncertainties are likely to remain.

5. Summary

Geological mapping of icy satellites poses problems not typically encountered in terrestrial mapping [*Wilhelms*, 1990], especially when the satellite has been dominated by tectonic processes. Initial mapping of Europa was based on Voyager data [*Lucchitta and Soderblom*, 1982]. Improved resolution and coverage from the Galileo mission have provided new insight into the complex geology of Europa and enable the definition of the basic units and structures for geological mapping. The ability to distinguish geologic units is typically based on characteristics such as surface morphology, texture, albedo, and color. The observation of these characteristics is influenced by illumination and viewing geometry, resolution, band-pass filters, and other parameters. Ideally, data for mapping would be obtained under uniform conditions. Because of limitations in the Galileo mission and the reconnaissance nature of the flybys, imaging data were taken under a wide range of conditions, especially in regard to scale and illumination. These limitations must be taken into account in the geologic mapping results.

The type localities for the material units and structures seen at various scales are given in Table 2. Table 3 gives the color scheme suggested for units on Europa; following this scheme will enable comparisons and synthesis among maps produced by the planetary community. Five primary units (i.e., three-dimensional materials comprising the ice-rich lithosphere) are recognized: plains, chaos, band, ridge, and crater-related materials. Mottled terrain as mapped on Voyager data appears to be composed of a variety of materials spanning a wide range of ages and is not recognized as a uniform geologic unit.

Plains materials are the most widespread unit on Europa. When observed at high resolution, most plains are seen to consist

of complex networks of crosscutting ridges and ridge sets. These are among the oldest materials recognizable on Europa, and are considered to represent a style of "tectonic resurfacing." Some plains observed at high resolution are relatively smooth and embay other terrains, suggesting relative youth and emplacement through cryovolcanic processes, such as the extrusion of melt onto the surface, or in situ mobilization of surface materials subjected to local heating.

Chaos material is characterized by terrain that has been severely disrupted and appears to have formed by the breakup of preexisting units. Two subunits are recognized, platy chaos, in which remnants of the plains units are visible as blocks within the chaos matrix, and knobby chaos, in which remnants of the former plains are not visible. Chaos materials are generally considered to represent the surface expression of subsurface activity, such as convection beneath the icy lithosphere, intrusion by diapirs, cryomagmatic processes, or localization of heat.

Band material is seen as linear, curvilinear, wedge-shaped, arcuate, and cuspate zones which have contrasting albedos and/or surface textures with respect to the surrounding terrain. Some band material exhibits a bilateral symmetry of surface characteristics, suggesting a complex pattern of spreading apart and infilling by younger material from the subsurface. Strike-slip displacements occur, evidenced by geometric relations of the band material and adjacent terrain. Ridge material constitutes linear to curvilinear positive relief features and can occur as single ridges, doublet ridges, or ridge complexes (two or more parallel ridges, segments of which may be discontinuous and/or anastomosing). At global scales, ridge material is too narrow to map as a material unit but can be shown with symbols. Ridge material appears to represent surficial deformation, possibly accompanied by emplacement of subsurface materials into the icy lithosphere or onto the surface. Some deformation could result from tidal stresses.

Numerous impact structures >10 km are recognized on Europa. Their material units include those associated with the crater interiors (rim, floor, and massif units), as well as possible ejecta deposits and secondary craters.

Structures, such as faults, and surface features, including scarps and troughs, are shown with conventional mapping symbols. Some landforms, such as domes and ridges, can be shown with symbols or as materials units, depending upon the scale of the mapping.

Acknowledgments. The authors wish to thank Jim Zimbelman and an anonymous reviewer for helpful comments. This investigation was supported by the Galileo project through contracts to the Solid State Imaging team from the Jet Propulsion laboratory. We thank Dan Ball for photographic support and Eddie Lo for computer support in this study.

References

Belton, M.J.S., et al., Galileo's first images of Jupiter and the Galilean satellites, *Science, 274*, 377-385, 1996.

Bierhaus, B., et al., Secondary cratering on Europa: A chronology of the Pwyll impact event and the Conamara region (abstract), *Eos Trans. AGU, 79(17)*, Spring Meet. Suppl., S198, 1998.

Carlson, R., R.E. Johnson, and M.S. Anderson, Sulfuric acid on Europa and the radiolytic sulfur cycle, *Science, 286*, 97-99, 1999

Carr, M.H., et al., Evidence for a subsurface ocean on Europa, *Nature, 391*, 363-365, 1998.

Chapman, C.R., et al., Populations of small craters on Europa, Ganymede, and Callisto: Initial Galileo imaging results, *Proc. Lunar Planet Sci. Conf. 28th*, 217-218, 1997.

Collins, G.C., J.W. Head III, R.T. Pappalardo, and N.A. Spaun, Evaluation of models for the formation of chaotic terrain on Europa, *J. Geophys. Res., 105*, 1709-1716, 2000.

Fagents, S., S.D. Kadel, R. Greeley, R.L. Kirk, and the Galileo SSI Team, Styles of cryovolcanism on Europa: Summary of evidence from the Galileo nominal mission, *Lunar Planet. Sci., XXIX*, 1721, 1998.

Fagents, S.A., R. Greeley, R.J. Sullivan, R.T. Pappalardo, and L.M. Prockter, Cryomagmatic mechanisms for the formation of Rhadamanthys Linea, triple band margins, and other low albedo features on Europa, *Icarus, 144*, 54-88, 2000.

Figueredo, P. H., and R. Greeley, Geologic mapping of the northern leading hemisphere of Europa from Galileo SSI data, *J. Geophys. Res.*, this issue.

Figueredo, P. H., K. S. Homan, R. Greeley, and the Galileo SSI Team, Latitudinal distribution of morphological units in an unexplored region of Europa, *Eos Trans. AGU, 79*(45), Fall Meet. Suppl., F541, 1998.

Figueredo, P. H., F. C. Chuang, R. Kirk, and R. Greeley, Evidence for a cryovolcanic origin of Europa's 'mitten' feature, *Lunar Planet. Sci.* [CD-ROM], *XXXI*, abstract 1026, 2000.

Geissler, P.E., et al., Evolution of lineaments on Europa: Clues from Galileo multispectral imaging observations, *Icarus 135*, 107-126, 1998a.

Geissler, P.E., et al., Evidence for non-synchronous rotation of Europa, *Nature, 391*, 368-370, 1998b.

Giese, B., R. Wagner, G. Neukum, R. Sullivan, and the SSI Team, Doublet ridge formation on Europa: Evidence from topographic data, *Am. Astron. Soc., Div. Planet. Sci. Annu. Meet. Abstr.*, 62.08, 1999a.

Giese, B., R. Wagner, and G. Neukum, The local topography of Europa: Stereo analysis of Galileo SSI images and implications for geology (abstract), *Geophys. Res. Abstr., 1*, 742, 1999b.

Golombek, M.P., and W.B. Banerdt, Constraints on the subsurface structure of Europa, *Icarus, 83*, 441-452, 1990.

Greeley, R., Geology of Europa: Galileo update, in *The Three Galileos: The Man, the Spacecraft, the Telescope*, edited by C. Barbieri et al., pp. 191-200, Kluwer Acad. Norwell, Mass., 1997.

Greeley, R., et al., Europa: Initial Galileo geological observations, *Icarus, 135*, 4-24, 1998.

Greenberg, R., et al., Tectonic processes on Europa: Tidal stresses, mechanical response, and visible features, *Icarus, 135*, 64-78, 1998.

Greenberg, R., G.V. Hoppa, B.R. Tufts, P. Geissler, J. Rigby, and S. Kadel, Chaos on Europa, *Icarus, 141*, 263-286, 1999.

Head, J.W., and R.T. Pappalardo, Brine mobilization during lithospheric heating on Europa: Implications for formation of chaos terrain, *J. Geophys. Res., 104*, 27,143-27,156, 1999.

Head, J.W., R. Pappalardo, G. Collins, R. Greeley, and the Galileo Imaging Team, Tectonic resurfacing on Ganymede and its role in the formation of grooved terrain, *Lunar Planet. Sci., XXVIII*, 535-536, 1997.

Head, J.W., N.D. Sherman, R.T. Pappalardo, R. Greeley, R. Sullivan, D.A. Senske, A. McEwen, and the Galileo Imaging Team, Geologic history of the E4 region of Europa: Implications for ridge formation, cryovolcanism and chaos formation, *Lunar Planet. Sci.* [CD-ROM], *XXIX*, abstract 1412, 1998.

Head, J.W., R. Pappalardo, and R. Sullivan, Europa: Morphological characteristics of ridges and triple bands from Galileo data (E4 and E6) and assessment of a linear diapirism model, *J. Geophys. Res., 104*, 24,223-24,235, 1999a.

Head, J.W., R.T. Pappalardo, L.M. Prockter, N.A. Spaun, G.C. Collins, R.Greeley, J. Klemaszewski, R. Sullivan, C. Chapman, and the Galileo SSI Team, Europa: Recent geological history from Galileo observations, *Lunar Planet. Sci.* [CD-ROM], *XXX*, abstract 1404, 1999b.

Head, J.W., R.T. Pappalardo, N.A. Spaun, L.M. Prockter, and G.C. Collins, Chaos terrain on Europa: Characterization from Galileo E12 very high resolution images of Conanmara Chaos, 2, Matrix, *Lunar Planet. Sci.* [CD-ROM], *XXX*, abstract 1587, 1999c.

Helfenstein, P., et al., Galileo observations of Europa's opposition effect, *Icarus, 135*, 41-63, 1998.

Hoppa, G., B.R. Tufts, R. Greenberg, and P. Geissler, Strike-slip faults on Europa: Global shear patterns driven by tidal stress, *Icarus , 141*, 287-298, 1999.

Kadel, S., S.A. Fagents, R. Greeley, and the Galileo SSI team, Trough-bounding ridge pairs on Europa – Considerations for an endogenic model of formation, *Lunar Planet Sci., XXIX*, 1078, 1998.

Kadel, S.D., F. Chuang, R. Greeley, J.M. Moore, and the Galileo SSI Team, Geological history of the Tyre region of Europa: A regional

perspective on Europan surface features and ice thickness, *J. Geophys. Res.*, this issue.

Klemaszewski, J.E., R. Greeley, L.M. Prockter, P.E. Geissler, and the Galileo SSI Team, Geologic mapping of Eastern Agenor Linea, Europa (abstract), *Lunar Planet. Sci.* [CD-ROM], *XXX*, abstract 1680, 1999.

Lucchitta, B.K., and L.A. Soderblom, The geology of Europa, in *Satellites of Jupiter*, edited by D. Morrison, pp. 521-555, Univ. of Ariz. Press, Tucson, 1982.

Lucchitta, B.K., L.A. Soderblom, and H.M. Ferguson, Structures on Europa, *Proc. Lunar Planet. Sci. Conf., 12B*, 1555-1567, 1981.

Malin, M.C., and D.C. Pieri, Europa, in *Satellites*, edited by J.A. Burns and M.S. Matthews, pp. 689-717, Univ. of Ariz. Press, Tucson, 1986.

McCord, T.B., et al., Salts on Europa's surface detected by Galileo's Near Infrared Mapping Spectrometer, *Science, 280*, 1242-1245, 1998.

McCord, T.B., et al., Hydrated salt minerals on Europa's surface from the Galileo near-infrared mapping spectrometer (NIMS) investigation, *J. Geophys. Res., 104*, 11,827-11,851, 1999.

Moore, J.M., et al., Large impact features on Europa: Results of the Galileo nominal mission, *Icarus, 135*, 127-145, 1998.

Neukum, G., Bombardment history of the Jovian system, in *The Three Galileos: The Man, the Spacecraft, the Telescope*, edited by C. Barbieri et al., pp. 201-212, Kluwer Acad., Norwell, Mass., 1997.

Pappalardo, R.T., Upward domes on Europa: Constraints on mottled terrain formation, *Lunar Planet. Sci.* [CD-ROM], *XXXI*, abstract 1719, 2000.

Pappalardo, R. T., and R. Sullivan, Evidence for separation across a gray band on Europa, *Icarus, 123*, 557-567, 1996.

Pappalardo, R.T., et al., Geological evidence for solid-state convection in Europa's ice shell, *Nature, 391*, 365-368, 1998.

Pappalardo, R.T., et al., Does Europa have a subsurface ocean? The (circumstanstial) geological evidence, *J. Geophys. Res., 104*, 24,015-24,056, 1999.

Patel, J.G., R.T. Pappalardo, L.M. Prockter, G.C. Collins, J.W. Head III, and the Galileo SSI Team, Morphology of ridge and trough terrain on Europa: Fourier analysis and comparison to Ganymede, *Eos Trans. AGU, 80*(17), Spring Meet. Suppl., S210, 1999.

Prockter, L.M., A.M. Antman, R.T Pappalardo, J.W. Head, and G.C. Collins, Europa: Stratigraphy and geological history of the anti-Jovian region from Galileo E14 solid-state imaging data, *J. Geophys. Res., 104*, 16,531-16,540, 1999a.

Prockter, L.M., R.T. Pappalardo, R. Sullivan, J.W. Head, J.G. Patel, B. Giese, R. Wagner, G. Neukum, and R. Greeley, Morphology and evolution of Europan bands: Investigation of a seafloor spreading analog, *Lunar Planet. Sci.* [CD-ROM], *XXX*, abstract 1900, 1999b.

Prockter, L.M., R.T. Pappalardo, and J.W. Head III, Strike-slip duplexing on Jupiter's icy moon Europa, *J. Geophys. Res., 105*, 9483-9488, 2000.

Schenk, P., and W.B. McKinnon, Fault offsets and lateral crustal movement on Europa: Evidence for a mobile ice shell, *Icarus, 79*, 75-100, 1989.

Senske, D.A., R. Greeley, J. Head, R. Pappalardo, R. Sullivan, M. Carr, P. Geissler, J. Moore, and the Galileo SSI Team, Geologic mapping of Europa: Unit identification and stratigraphy at global and local scales, *Lunar Planet. Sci., XXIX*, abstract 1743, 1998.

Shoemaker, E.M., and R.J. Hackman, Stratigraphic basis for a lunar time scale, in *The Moon*, edited by Z. Kopal and Z.K. Mikhailov, pp. 289-300, Academic, San Diego, Calif., 1962.

Smith, B.A., et al., The Jupiter system through the eyes of Voyager 1, *Science, 204*, 951-972, 1979a.

Smith, B.A., et al., The Galilean Satellites and Jupiter: Voyager 2 imaging science results, *Science, 206*, 927-950, 1979b.

Spaun, N.A., J.W. Head, G.C. Collins, L.M. Prockter, and R.T. Pappalardo, Conamara Chaos Region, Europa: Reconstruction of mobile polygonal ice blocks, *Geophys. Res. Lett., 25*, 4277-4280, 1998.

Spaun, N.A., L.M. Prockter, R.T. Pappalardo, J.W. Head III, G.C. Collins, A. Antman, R. Greeley, and the Galileo SSI Team, Spatial distribution of lenticulae and chaos on Europa, *Lunar Planet. Sci.* [CD-ROM], *XXX*, abstract 1847, 1999.

Spudis, P., and R. Greeley, Surficial geology of Mars: A study in support of a penetrator mission to Mars, *NASA Tech. Memo. TM X-73,184*, 54 pp., 1976.

Sullivan, R., et al., Episodic plate separation and fracture infill on the surface of Europa, *Nature, 391*(22), 371-373, 1998.

Sullivan, R., R. Greeley, J. Klemaszewski, J. Moreau, B.R. Tufts, J.W. Head III, R. Pappalardo, and J. Moore, High resolution geological mapping of ridged plains on Europa, *Lunar Planet. Sci.* [CD-ROM], *XXX*, abstract 1925, 1999.

Tanaka, K.L., et al., *The Venus Geologic Mappers Handbook, U.S. Geol. Surv. Open File Rep., 94-438*, 66 pp., 1994.

Tufts, B.R., R. Greenberg, G. Hoppa, and P. Geissler, Astypalaea Linea: A large-scale strike-slip fault on Europa, *Icarus, 141*, 53-64, 1999.

Tufts, B.R., R. Greenberg, G. Hoppa, and P. Geissler, Lithospheric dilation on Europa, *Icarus*, in press, 2000.

Turtle, E.P., H.J. Melosh, and C.B. Phillips, Tectonic modeling of the formation of Europan ridges, *Eos Trans. AGU, 79*(45) Fall Meet. Suppl., F541, 1998.

Wilhelms, D.E., Geologic mapping of the second planet, *U.S. Geol. Surv. Interagency Report, Astrogeology, 55*, 1972.

Wilhelms, D.E., Geologic mapping, in *Planetary Mapping*, edited by R. Greeley and R.M. Batson, pp. 208-260, Cambridge Univ. Press, New York, 1990.

Williams, D.A., et al., Terrain variation on Europa: Overview of Galileo orbit E17 imaging results, *Lunar Planet. Sci* [CD-ROM], *XXX*, abstract 1396, 1999.

Williams, K.K., and R. Greeley, Estimates of ice thickness in the Conamara Chaos region of Europa, *Geophys. Res. Lett., 25*, 4273-4276, 1998.

Wilson, L., and J.W. Head, Cryomagmatism: Processes of generation, ascent and eruption and applications to Europa, *Lunar Planet. Sci.* [C-ROM], *XXX*, abstract 1689, 1999.

Zahnle, K., L. Dones, and H. Levison, Cratering notes on the Galilean satellites, *Icarus, 136*, 202-222, 1998.

M.J.S. Belton, National Optical Astronomy Observatories, Tucson, AZ 85726-6732.

F C. Chuang, P.H. Figueredo, R. Greeley, S.D. Kadel, J.E. Klemaszewski, and D.A. Williams, Department of Geology, Ariz State Univ., Physical Sciences F-556, Tempe, AZ 85287-1404. (greeleyatasu.edu)

G.C. Collins, J.W. Head III, R.T. Pappalardo, L.M. Prockter, and N.A. Spaun, Department of Geological Sciences, Brown University, Providence, RI 02912.

T.V. Johnson and D.A. Senske, Jet Propulsion Laboratory, 4800 Oak Grove Drive, Pasadena, CA 91109.

J.M. Moore, NASA Ames Research Center, MS 245-3, Moffett Field CA 94035-1000

R J. Sullivan, Center for Radiophysics and Space Physics, Cornell Univ., 308 Space Sciences Building, Ithaca, NY 14853.

K.L. Tanaka, U.S. Geological Survey, 2255 North Gemini Drive, Flagstaff, AZ 86002.

B.R. Tufts, Lunar and Planetary Lab, Univ. of Ariz., Tucson, AZ 85721.

(Received September 3, 1999; revised May 10, 2000;
accepted May 11, 2000)